



Integrated Low Carbon H₂ Conversion with In-Situ Carbon Mineralization from Aqueous Biomass Oxygenate Precursors by Tuning Reactive Multiphase Chemical Interactions

Journal:	<i>Reaction Chemistry & Engineering</i>
Manuscript ID	RE-ART-12-2022-000542.R1
Article Type:	Paper
Date Submitted by the Author:	09-Mar-2023
Complete List of Authors:	Ochonma, Prince; Cornell University Noe, Christopher; Cornell University Mohammed, Sohaib; Cornell University, Civil and Environmental Engineering Mamidala, Akanksh; Cornell University Gadikota, Greeshma; Cornell University,

1
2
3
4
5
6
7
8
9
10
11
12
13
14
15
16

***Integrated Low Carbon H₂ Conversion with In-Situ Carbon
Mineralization from Aqueous Biomass Oxygenate Precursors by
Tuning Reactive Multiphase Chemical Interactions***

*Prince Ochonma,¹ Christopher Noe,² Sohaib Mohammed,³ Akanksh Mamidala,³
and Greeshma Gadikota^{1,3*}*

¹Robert Frederick Smith School of Chemical and Biomolecular Engineering, Cornell University, 113 Ho Plaza, Ithaca, NY 14853

²Department of Chemistry, College of Art and Science, Stony Brook University, Stony Brook, NY 11790

³School of Civil and Environmental Engineering, Cornell University, 527 College Avenue, 117 Hollister Hall, Ithaca, NY 14853

* Corresponding Author. Phone: +1 607-255-4796. E-mail: gg464@cornell.edu

1 Abstract

2 Meeting our rising demand for clean energy carriers such as H₂ from renewable biomass resources
3 is challenged by the co-emission of CO₂ and CH₄. To address this challenge, we design novel
4 reactive separation pathways that integrate multiphase chemical reactions by harnessing Ca & Mg
5 bearing minerals as a sorbent to capture CO₂ released during the hydrothermal deconstruction of
6 aqueous biomass oxygenates to produce H₂ and solid carbonates via low temperature aqueous
7 phase reforming and thermodynamically downhill carbon mineralization. Earth abundant catalysts
8 such as Ni/Al₂O₃ are effective in producing H₂ yields as high as 79% and 74% using ethylene
9 glycol and methanol in the presence of Ca(OH)₂ as the alkaline sorbent, without contaminating or
10 deactivating the catalyst. H₂ yields with in-situ carbon mineralization using Ni or Pt/Al₂O₃ catalyst
11 are enhanced based on the following order of reactivity: acetate < glycerol < methanol < formate
12 < ethylene glycol. These studies demonstrate that the multiphase chemical interactions can be
13 successfully tuned to enhance H₂ yields through the selective cleavage of C-C bonds using
14 Ni/Al₂O₃ catalysts to deconstruct biomass oxygenates for producing H₂ and CO₂, and *in-situ*
15 carbon mineralization by harnessing abundant alkaline materials, as demonstrated using ladle slag.
16 This approach unlocks new scientific possibilities for harnessing multiple emissions including
17 abundant organic-rich wastewater streams and alkaline industrial residues to co-produce low
18 carbon H₂ and carbonate-bearing materials for use in construction by using renewable solar
19 thermal energy resources.

20 **Keywords:** H₂ conversion, *in-situ* carbon mineralization, oxygenates, aqueous phase reforming,
21 biomass & wastewater valorization, multiphase chemical interactions.

22

1

2 **1. Introduction**

3 Advancing sustainable low carbon chemical pathways for meeting our energy needs while limiting
4 detrimental impacts on climate and the environment is our societal and scientific grand challenge.¹

5 One emerging approach to realize rapid decarbonization is by harnessing hydrogen as a sustainable
6 and clean energy carrier^{2,3} for use in industrial processes, fuel cells, transportation, and heating.

7 Hydrogen generated with inherent carbon removal and via electrolysis of water resources has the
8 potential to decarbonize sectors which pose a challenge to abating CO₂ emissions such as aviation,

9 long distance transportation, and shipping which contributes to ~ 2.2 Gt of CO₂ emissions
10 annually.¹ Current methods for producing hydrogen at commercial scales requires energy-

11 intensive, high-temperature steam methane reforming (SMR) of non- renewable feedstocks which
12 results in significant CO₂ emissions.⁴ SMR for H₂ production contributes to about 3% of global

13 CO₂ emissions annually (~1200 MMT of CO₂ per year).⁵ Despite the promise of H₂ generation
14 via water electrolysis (also known as green electrolysis), significant scientific and technological

15 advances are needed to achieve favorable economics for scalable deployment.⁶

16

17 One of the less explored but highly promising approaches is to harness low value and renewable
18 aqueous biomass oxygenates such as bio-derived methanol, ethylene glycol, ethanol, formate and

19 acetate for producing H₂.^{4,7-9} Depending on the sourcing and processing conditions, the use of
20 aqueous bio derived feedstocks for H₂ production has the potential to be carbon neutral.¹⁰ Bio-

21 derived oxygenates are abundant in wastewater from biomass processing. For instance, bio-
22 methanol, glycerol, and ethylene glycol are major by-products of bio-based fuels processing.^{11,12}

23 In 2020, about 1,817 million gallons of biodiesel was produced in the United States.¹³ Every

1 gallon of biodiesel produced generates approximately 1.05 pounds of glycerol.¹⁴ Formate and
2 acetate are produced in massive quantities from the anaerobic digestion of food waste and
3 wastewater sludge.^{15,16} Upcycling aqueous biomass oxygenates to produce H₂ is a less
4 conventional but a unique approach that valorizes these waste streams and enhances resource
5 utilization as opposed to treating it as a waste in need of remediation.

6
7 Approaches to produce H₂ from aqueous biomass oxygenates at 200-300°C in pressurized N₂
8 environments in the presence of a metal catalyst^{8,17} have resulted in high H₂ yields. However, in
9 this process, which is also known as Aqueous Phase Reforming (APR), H₂ evolution is
10 accompanied by the co-generation of CO₂. One scientific challenge in APR lies in enabling the
11 cleavage of C-C bonds to promote H₂ and CO₂ evolution as opposed to C-O bond cleavage which
12 results in CH₄ formation. This challenge has been resolved by using catalysts such as Ni and Pt
13 which have shown to favor the cleavage of C-C bonds.^{8,17} One of the key advantages of this
14 approach is that the water content co-present with biomass oxygenates can be synergistically
15 harnessed for H₂ conversion. Potentially limiting reaction kinetics and thermodynamics due to
16 elevated pressures and hydrothermal conditions are overcome by harnessing catalysts to
17 selectively cleave biomass oxygenate molecules. In contrast to conventional biomass gasification
18 which occurs at temperatures >500°C,¹⁸ this approach harnesses significantly lower temperatures
19 in the range of 200-250°C which can be achieved using renewable solar thermal energy
20 resources.¹⁹

21
22 To date, research conducted on enhancing H₂ yields from aqueous biomass oxygenates has focused
23 on the role of catalysts in enhancing reactivity. For example, Vaidya and Lopez-Sanchez⁸

1 summarized the influence of group VIII metal catalysts such as Ni and Pt on metal oxide supports
2 (e.g., Al_2O_3) in aiding the C-C cleavage of biomass oxygenate molecules to produce H_2 and CO_2 .
3 Extensive studies have been conducted on harnessing biomass oxygenates such as glycerol,²⁰
4 sorbitol,²¹ xylitol,²² methanol,¹⁷ ethanol,²³ acetic acid,²⁴ and butanol²⁵. Conversion of 10–60 wt.%
5 aqueous feed concentrations of glucose,²¹ cellulose,²⁶ and glycols²⁷ have been reported,
6 demonstrating that this process is also effective for converting non-volatile biomass feedstocks
7 into H_2 . Despite the promise of aqueous phase reforming, H_2 selectivity remains a challenge.
8 Competing methanation reaction which involves the reaction of H_2 and CO/CO_2 ⁸ to produce CH_4
9 limits H_2 yield and selectivity. Slower kinetics at lower temperatures in the range of 200–250°C as
10 opposed to temperatures greater than 500°C may limit H_2 yields due to the endothermic nature of
11 biomass deconstruction pathways.²⁸ In addition to H_2 selectivity and kinetic limitations, significant
12 quantities of CO_2 are co-produced, which implies that an additional unit for separation and
13 purification of gas streams is essential to produce low carbon H_2 . Thus, novel chemical pathways
14 need to be designed for highly selective, energy- and atom-efficient reactive separation of CO_2
15 integrated with H_2 conversions from aqueous biomass oxygenate precursors.

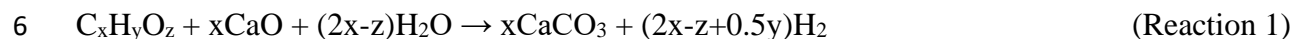
16

17 Several approaches exist for CO_2 capture and removal post energy and resource conversion
18 processes. CO_2 capture involves separating CO_2 in dilute flue gas streams to produce a CO_2 -rich
19 stream and CO_2 -lean streams using adsorbents, absorbents, and membranes.^{29–31} Furthermore,
20 approaches to remove CO_2 via carbon mineralization obtained post CO_2 capture have been
21 investigated. Carbon mineralization is a thermodynamically downhill pathway for converting
22 gaseous CO_2 into solid carbonates. Specifically, pH swing approaches in which acids are used to
23 facilitate the dissolution of alkaline-bearing minerals and residues followed by bases to enhance

1 carbonate concentrations for solid carbonate formation, have been well established.³² As an
2 alternative to these carbon mineralization pathways, single step approaches in which regenerable
3 solvents are used to enhance CO₂ capture and mineralization to produce solid carbonates which
4 results in the chemical regeneration of the solvents^{30,33,34} has been shown to be very effective
5 without the need for external reagents for pH swing.

6
7 While post combustion CO₂ capture and mineralization has been shown to be effective, integration
8 of H₂ conversion with CO₂ mineralization remains less explored. Coupling thermodynamically
9 downhill carbon mineralization pathways with uphill energy and resource conversions has the net
10 impact of lowering the overall energy needs while contributing to inherent carbon removal. For
11 example, coupling the water gas shift reaction with carbon mineralization of Ca- and Mg-silicates
12 is favored by elevated temperatures in the range of 150-250°C and pressurized gaseous
13 environments.³⁵ This approach is inspired by evidence of more than 80% conversion of olivine
14 ((Mg, Fe)₂SiO₄) to magnesium carbonate at elevated partial pressures of CO₂ in the range of 100-
15 150 atm and temperatures in the range of 150 - 185°C.³⁶ Enhanced H₂ yields with inherent carbon
16 removal via mineralization remains less explored in the context of using aqueous biomass
17 oxygenates. The conditions that favor carbon mineralization including elevated temperatures, high
18 CO₂ partial pressures and aqueous slurry environments are well-aligned with the deconstruction
19 of biomass oxygenates to produce H₂ with inherent removal of CO₂. Elevated temperatures
20 increases the reactivities of Ca- and Mg-oxides, hydroxides, and silicates³⁷ and enhance the
21 precipitation of solid Ca- and Mg-carbonates whose solubility decreases with increasing
22 temperature³⁸ The high pressure at which these reactions proceeds also implies enhanced CO₂
23 capture rates, due to increased CO₂ solubility.³⁹

1 In a prior study, we showed that suppression of methane formation using catalysts and the presence
2 of alkaline resources (e.g., calcium oxide) to capture CO₂ are effective in enhancing H₂ yields from
3 bio-derived aqueous feedstocks such as ethanol, methanol, glycerol, ethylene glycol, acetone, and
4 acetic acid.²⁸ The reaction representing enhanced H₂ yield with inherent carbon removal is as
5 follows:



7 The proposed *in-situ* CO₂ capture approach from aqueous biomass oxygenate resources does not
8 require expensive separation of CO₂, utilizes enormous quantities of available feedstocks, and can
9 be integrated into existing biorefineries. A key consideration is the suppression of methane
10 evolution using a catalyst such as Pt or Ni. Platinum supported on alumina has been shown to
11 result in high yield and selectivity of H₂.²⁷ As an alternative to catalysts synthesized from precious
12 metals, nickel-bearing catalysts have been proposed as an economical alternative. Low H₂
13 selectivity in the presence of Ni-based catalysts¹⁷ motivated research efforts to dope these catalysts
14 with Cu, Ce and Sn and use various metal oxides and carbonaceous materials as supports to
15 enhance H₂ selectivity.⁴⁰⁻⁴²

16

17 Prior work showing the thermodynamic feasibility of enhancing H₂ yields with inherent carbon
18 removal from aqueous biomass oxygenates using calcium oxide has opened new possibilities for
19 harnessing alkaline industrial residues bearing calcium oxide. Among alkaline industrial residues,
20 ladle slag (LS) generated as a by-product of post-processing molten steel produced from the EAF
21 steel making process has a significant potential to store CO₂ due to its high calcium and magnesium
22 content.⁴³ However, large quantities of these residues still end up in landfills with significant
23 disposal costs and detrimental environmental impacts. The valorization potential of these materials

1 is low due to their weak cementitious properties, low strength, and potential leaching of heavy
2 metals which can inhibit utilization for several key applications.⁴⁴ Accelerated carbon
3 mineralization of ladle slag can upgrade their chemical and mechanical properties which is
4 beneficial to subsequent utilization as construction materials in blended cement or
5 concrete.^{44,45} Incorporating compositions as low as 10 wt% of carbonate-bearing steel slag in
6 construction materials has shown to enhance the compressive strength from about 33–50 MPa³³
7 Recent studies have reported that the heavy metal immobilization potential can also be enhanced
8 by carbon mineralization.^{44,46} The direct use of alkaline industrial residues rich in Ca- or Mg-
9 oxides and hydroxides circumvents the need to produce high purity Ca- or Mg- oxides and
10 hydroxides for carbon mineralization. The proposed approach contributes to the upcycling of
11 multiple low-value streams including aqueous biomass oxygenates and ladle slag to produce H₂
12 with inherent carbon removal and can establish a waste-to-resource supply chain for advancing a
13 low carbon H₂ economy, as shown in **Figure 1**.

14
15 Despite the promising potential of these pathways to produce H₂ with inherent carbon removal,
16 several open scientific challenges remain. First, the kinetics and mechanisms associated with
17 enhanced H₂ recovery with inherent carbon removal from biomass oxygenates remain unresolved.
18 Second, the hypothesis that nickel-bearing catalyst can be effective in enhancing H₂ yields with
19 inherent carbon removal as an alternative to platinum-bearing catalyst, has not been investigated.
20 Third, the effectiveness of various reaction modes in enhancing H₂ yield and selectivity such as
21 those in which the alkaline residues, catalysts and oxygenates are co-present in the aqueous phase
22 (referred to as Mode I in this study) versus placing the alkaline residue in the gas phase while the
23 biomass oxygenates, and catalysts are in the aqueous phase (referred to as Mode II in this study)

1 has not been studied. Fourth, the enhancement in H₂ yield and selectivity associated with using
2 alkaline industrial residues such as ladle slag has not been contrasted with that of pure calcium
3 hydroxide. Fifth, the mechanisms associated with the deconstruction of biomass oxygenates and
4 associated reactivity based on their structure has not been elucidated. Sixth, identification of the
5 rate limiting step in multiphase chemical transformations is not trivial. In the context of enhanced
6 H₂ recovery with inherent carbon removal, biomass deconstruction, selective H₂ formation over
7 CH₄ evolution, CO₂ solubility, or the conversion of CO₂ to solid carbonate could be rate limiting.
8 Identifying the rate limiting step is crucial for developing approaches to accelerate low carbon H₂
9 recovery. Therefore, the aim of this study is to elucidate the mechanisms and rates of enhanced H₂
10 production with inherent carbon removal from aqueous biomass oxygenates such as methanol,
11 ethylene glycol, acetate, formate, and glycerol using calcium hydroxide as the alkaline sorbent.
12 The effectiveness of using ladle slag for in-situ carbon capture is investigated.

13
14 The proposed approach of harnessing low value aqueous biomass oxygenates for enhanced H₂
15 yield with inherent carbon removal is transformative. This approach adds to the portfolio of
16 technologies for Bioenergy with Carbon Capture and Storage (BECCS) which involves harnessing
17 bioenergy while capturing and storing biogenic CO₂.⁴⁷ In 2018, IPCC reported that BECCS can
18 contribute to carbon offsets to the order of ~ 0.5 – 5 GtCO₂/year with costs in the range of \$ 100 -
19 \$ 200/ton of CO₂.⁴⁸ These estimates were based on conventional BECCS technologies where
20 biomass is co-fired with coal in a power plant and the captured CO₂ is stored in a subsurface
21 geologic environment. The proposed approach of producing H₂ with inherent carbon removal from
22 aqueous biomass oxygenates eliminates the need for *in-situ* CO₂ storage and monitoring over long
23 periods of time. Advances in solar thermal energy technologies facilitate distributed conversion of

1 aqueous biomass oxygenates to H₂ with inherent carbon removal. Fundamental mechanistic
2 insights into the deconstruction of aqueous biomass oxygenates to produce low carbon H₂
3 developed through this study are crucial for the scalable realization of these pathways for
4 implementation.

5 **2. Materials and Methods**

6 **2.1 Materials**

7 High purity oxygenates such as methanol (99.9%, Thermo Fisher Scientific), glycerol (99.5%,
8 Thermo Fisher Scientific), ethylene glycol (99.7%, Thermo Fisher Scientific), sodium acetate
9 (99%, Fisher Bioreagents), and sodium formate (99.9% Acros Organics) are used as model
10 wastewater bio-oxygenates in this study. Platinum (Pt) and nickel (Ni) on alumina (Al₂O₃) support
11 were used as catalyst in these experiments. Pt/Al₂O₃ catalyst with a composition of 5 wt.% is
12 obtained from Sigma Aldrich. Ni/Al₂O₃ catalyst with a composition of 5 wt. % is synthesized in
13 the lab via the incipient wetness impregnation method. To synthesize Ni/Al₂O₃ catalyst, γ-Al₂O₃
14 (Strem Chemicals Inc., 97%) is impregnated with a solution bearing Ni(NO₃)₂·6H₂O (Thermo
15 Fisher Scientific). Post impregnation, the samples are dried at 80 °C, and then calcined or reduced
16 in flowing N₂ or H₂ (95%:5%) gas stream at 450 °C (± 5 °C) for 5 hours. Calcium hydroxide
17 (Thermo Fisher Scientific), and Ladle Slag (LD) from Nucor's Electric Arc Furnace (EAF) steel
18 making plant in Auburn, NY are used as the alkaline sorbents for this study.

19 *Elemental Analysis of Ladle Slag*

20 The major constituent compositions of ladle slag used as an alkaline sorbent in this study are
21 determined using Wavelength Dispersion X-Ray Fluorescence (WD-XRF, Panalytical Axios).
22 Prior to elemental analyses, the samples are crushed and pulverized followed by the formation of

1 a homogenous glass disk by the fusion of the sample and a lithium tetra- borate/lithium metaborate
2 mixture. The Loss on Ignition (LOI) is determined separately and gravimetrically at 1000°C. The
3 prepared disks are analyzed by Wavelength Dispersion X-Ray Fluorescence (WD-XRF). The LOI
4 is included in the matrix correction calculations, which are performed by the XRF software. X-
5 Ray Photoelectron Spectroscopy (XPS, Scienta Omicron ESCA-2SR, Al K α) surface analysis and
6 Inductively Coupled Plasma Optical Emission Spectrometry are utilized to confirm the weight
7 ratio of Ni and Pt metals to Al₂O₃ support used in this study as shown in **Figure S1**.

8 *Determination of the chemical composition of the solid samples*

9 The thermal behavior of the alkaline sorbents and their reacted products are determined using a
10 Thermo Gravimetric Analyzer (TGA, Discovery SDT 650, TA instrument), and Total Carbon
11 Analysis (TCA, LECO CS 844). In a typical TGA run, samples are exposed to a N₂ environment
12 (flow rate: 50 ml/min) as the temperature is ramped from 25 °C to 1000 °C at a rate of 10 °C /min.
13 Based on the weight drop related to each dehydroxylation or calcination temperature, the carbonate
14 phase in the solid sample is identified and the extent of carbon mineralization is determined.
15 Detailed information on the estimation of the extent of carbonation can be found in the
16 supplementary information. During the TCA run, samples are placed in a ceramic boat and
17 combusted in the presence of O₂ at temperatures as high as 1000 °C. The combustion process
18 converts all carbon – both inorganic and organic – into CO₂ and CO, and the total carbon is
19 reported. In this study both the TCA mode and TGA techniques are used to estimate the extents of
20 carbon mineralization, and the results of both methods are compared to assess consistency. The
21 crystalline phases present in alkaline sorbents, catalysts and reaction products are detected using
22 X-ray diffraction (XRD, Bruker D8 Advance ECO powder diffractometer, Bruker with Cu K α

1 radiation (40 kV, 25 mA)). The samples are scanned over the 2θ range from 20° to 80° . The FTIR
2 spectra of powder and liquid samples are recorded with a FTIR spectrometer (ThermoFisher
3 Scientific). Thirty-two scans are collected for each measurement in the spectral range of 4,000–
4 400 cm^{-1} with a resolution of 4 cm^{-1} and the average was taken as a representative measurement.
5 **Figure S2a** represents the FTIR spectra corresponding to various oxygenates for a baseline
6 comparison.

7 *Determination of the morphological features of the solid samples*

8 The particle size distributions of the materials are determined using a particle size analyzer (Anton
9 Paar). **Figure S3 (a)** represents the particle size distribution of ladle slag. The pore size
10 distributions (PSD) surface areas, and pore volumes of starting materials, and synthesized particles
11 are determined from N_2 adsorption-desorption isotherms using the Brunauer–Emmett–Teller
12 technique (BET) (Quantachrome Autosorb iQ Analyzer, Boynton Beach, FL). Before measuring
13 the adsorption-desorption isotherms, the synthesized samples are outgassed at 120°C for 24 h.
14 The total pore volume, average pore diameters and pore size distributions are obtained from the
15 N_2 adsorption branches of isotherms using the Barrett–Joyner–Halenda (BJH) method.

16 *Determination of the chemical compositions of liquids using NMR spectroscopy*

17 The compositions of the oxygenate molecules are determined using Nuclear Magnetic Radiation
18 (NMR). NMR data are acquired on a 500 MHz Bruker AVIII spectrometer equipped with a
19 Prodigy BBO probehead. To calculate mass composition, ^1D and ^1H spectra are acquired with 4
20 scans, 30 seconds relaxation delay, 10 kHz spectral width, and 3.3 s acquisition time. The spectra
21 are processed in MNova (version 14.2.3, Mestrelab Research S.L.). The FID are zero filled to 128k

1 points prior to Fourier transform. Automatic phase correction is applied followed by baseline
2 correction with 5th-order Bernstein polynomials. Spectra are superimposed, and frequency aligned
3 using solute signals, and integrated using automatic linear correction for solute signals. Minor
4 products are identified by suppressing the water signal using WET as implemented in TopSpin
5 3.6.4 (Bruker BioSpin). WET-1H spectra are acquired with 64 scans, 3 seconds relaxation delay,
6 8 kHz spectral width, and 2 s acquisition time. **Figure S2b** represents the NMR spectra
7 corresponding to various oxygenates for a baseline comparison.

8 **2.2** *Experimental Setup*

9 The experiments to investigate enhanced H₂ recovery from aqueous biomass oxygenates are
10 conducted in a stainless-steel stirred reactor (Micro Bench Top Reactor, Parr Instrument
11 Company), maintained at a temperature of 240 °C (± 5 °C), 50 bar (± 1 bar) N₂ pressure, and stirring
12 rate of 10 rpm (± 2 rpm). **Figure 2 (a)** shows a schematic representation of the reactor system.
13 Aqueous biomass oxygenates with a composition of 3 wt.% are prepared by mixing high purity
14 oxygenates in an appropriate volume of distilled water, and 3 g (± 0.05 g) of either Ni or Pt on
15 alumina catalyst is used in the experiments that required a catalyst. Experiments are also performed
16 without a catalyst as the base case. Prior to the start of each experiment, the system is purged with
17 N₂ for 3–5 min to remove any trapped gas impurities. The system is then heated, and the gas
18 pressure is set to the desired value. The start of the reaction is marked by reaching the desired
19 temperature setpoint of 240 °C (± 5 °C). At the end of the reaction, the reactor is cooled back to
20 room temperature, and the products are collected and analyzed.

21 The product gases are analyzed by connecting the reactor to a gas chromatograph (GC) equipped
22 with four columns connected in series (MS and Poraplot Q) with thermal conductivity and flame

1 ionization detectors (TCD-FID). H₂, O₂, and N₂, CH₄ and CO were analyzed using Channel A with
2 a molecular sieve column and argon as the carrier gas; CO₂, C₂H₄, and C₂H₆ are analyzed using
3 Channel B with a molecular sieve column and helium as the carrier gas. The gas sample is injected
4 after every experiment is completed. Since the concentration of inert gas, N₂, is already known at
5 the start of the reaction, the concentrations of product gases are calculated based on the N₂
6 concentration in the gas samples. For each reaction condition, an error bar is generated by using
7 three to four repeated experiments. The gas yields are obtained by GC analysis and their purities
8 are calculated by volume concentration ratio. Known concentrations of standard gases i.e., H₂, CO,
9 CO₂, and hydrocarbon gases are used as calibration gases.

10 H₂ evolution is also studied by exploring two distinct modes of operation. In Mode I, the biomass
11 oxygenates, alkaline sorbent (calcium hydroxide), and catalyst are co-present as a slurry. In Mode
12 II, a basket bearing the alkaline sorbent is in contact with the gas phase and the fluid phase
13 (oxygenate-water mixture) remains in contact with the catalyst. Placing the catalyst in the aqueous
14 phase and the alkaline sorbent in the gas phase enables ease of recovery and reuse of the catalyst.
15 The hypothesis that reactivities will differ in modes I and II due to differences in mass transfer
16 behavior is investigated. For example, in Mode II, CO₂ ex-solution into the gas phase is essential
17 for *in-situ* CO₂ capture unlike in Mode I, where CO₂ in the aqueous phase can be directly captured
18 to produce solid carbonates. In both modes, the solid products were recovered and separated from
19 the liquid mixture using vacuum filtration and dried in a vacuum oven. The recovered solids were
20 analyzed for carbonate content, and their structural and morphological features. The liquid
21 products and catalysts before and after reactions are also characterized to determine changes in
22 chemical composition.

2.3 *Extent of carbon mineralization and product yield calculations*

The extent of carbon mineralization is defined as the measured amount of CO₂ stored in the samples as solid carbonate relative to the theoretical maximum CO₂ storage capacity based on the stoichiometry of complete conversion and is expressed by Eq. (1):

$$\text{Extent of carbon mineralization (\%)} = \frac{\text{measured amount of CO}_2 \text{ in the samples}}{\text{theoretical maximum CO}_2 \text{ storage capacity}} \times 100 \quad (1)$$

More information on chemical phase determination and extent of carbon mineralization of heterogenous slag samples can be found in the supplementary information.

The conversion of biomass oxygenates and associated yields of products (e.g., H₂, CO, CH₄, and CO₂) are determined using Eq. 4-6 as shown below.

$$\% \text{ Conversion of Biomass Oxygenates (BO)} = \frac{\text{BO}_{\text{in}} - \text{BO}_{\text{out}}}{\text{BO}_{\text{in}}} * 100 \quad (4)$$

$$\% \text{ H}_2 \text{ yield} = \frac{\text{Moles of H}_2 \text{ produced}}{\text{Moles of biomass oxygenate fed} * \text{Stoichiometric Ratio (SR)}} * 100 \quad (5)$$

$$\% \text{ CO, CO}_2 \text{ and alkanes yield} = \frac{\text{Moles of C in compound produced}}{\text{Moles of C atoms in BO fed}} * 100 \quad (6)$$

Stoichiometric ratio (SR) is a factor obtained from the stoichiometry for complete conversions of biomass oxygenates as shown in **Table S1** in the supporting information.

3. Results and Discussion

3.1 *Pathways involved in enhanced H₂ recovery with inherent carbon removal from aqueous biomass oxygenates*

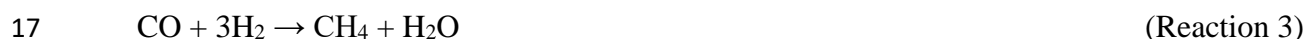
The three key multiphase reactions involved in producing H₂ with *in-situ* CO₂ capture from aqueous biomass oxygenates are: (i) the deconstruction of the oxygenates over a metal catalyst, (ii) the selective cleavage of C-C or C-O cleavage to produce CO/H₂/CO₂ and CH₄ over a metal

1 catalyst, respectively, and (iii) the reactivity of CO₂ with Ca- or Mg-oxides or hydroxides to
2 produce Ca- or Mg-carbonates. Robust characterization of multiphase gas-liquid-solid chemical
3 interactions are crucial for delineating which of these steps is rate-limiting.^{28,49} In the first step, the
4 oxygenates typically undergo reversible dehydrogenation over a metal catalyst to produce
5 adsorbed intermediates, prior to cleavage of C-C and C-O bonds. The reaction pathways involved
6 in the deconstruction of aqueous biomass oxygenates are shown in **Figure 2 (b)**.

7
8 When considering the deconstruction mechanisms of glycerol and ethylene glycol, the first
9 pathway usually involves the cleavage of the C–C bond leading to the formation of CO and H₂.
10 This pathway is ideal for producing adsorbed CO for water gas shift reactions in the subsequent
11 step. However, when the starting feedstock is acetate, the cleavage of the C-C bond typically leads
12 to the formation of CO, H₂ and CH₄. Another reaction pathway involves the cleavage of C-O bonds
13 followed by hydrogenation with ethylene glycol and glycerol precursors to produce an alcohol.
14 The alcohol can further react on the metal surface via adsorption, C-C bond cleavage or C-O bond
15 cleavage which can lead to the formation of CH₄, CO₂, H₂ and H₂O. Another possible pathway
16 involves the desorption of species from the metal surface followed by rearrangement (which may
17 occur on the catalyst support and/or in the aqueous phase) to form an acid, which can then undergo
18 surface reactions including adsorption, C-C bond cleavage, and C-O bond cleavage to form alkanes
19 (e.g., CH₄, C₂H₆), CO₂, H₂ and H₂O. These interactions highlight selectivity challenges that exist
20 in tuning multiphase chemical interactions for preferentially synthesizing CO, CO₂, and H₂ over
21 alkanes or alcohols. It has been shown that slightly acidic solutions promote alkane formation due
22 to acid-catalyzed dehydration reactions, followed by hydrogenation on the metal interface. In
23 contrast, neutral and basic solutions yield high H₂ and low alkane selectivities⁴⁹ Therefore, the

1 hypothesis that alkaline environments bearing calcium hydroxide or oxide aid the selective
2 deconstruction of biomass oxygenates to produce H₂, is investigated in this study.

3
4 The second potentially rate-limiting step involves the selectivity of gas phase chemical reactions
5 to produce CO₂ and H₂ via the water gas shift reaction (see Reaction 2) as opposed to methanation
6 reactions (see Reactions 3 and 4) which result in CH₄ evolution. Methanation reactions scavenge
7 H₂ to produce CH₄, which is not desirable. Examples of other possible reactions that limit H₂ yields
8 include alcohol dehydration which produces large amounts of hydrocarbons, CO/CO₂ reduction
9 and Boudouard reactions which leads to the formation solid carbon.²⁸ Acidic environments arising
10 from the evolution of CO₂ and dissolution aids methanation. However, the hypothesis that alkaline
11 environments such as the presence of Ca(OH)₂ aids CO₂ removal and suppresses methane
12 evolution has not been extensively explored. Furthermore, according to the Le Chatelier
13 principle,⁵⁰ the removal of CO₂ promotes an equilibrium shift in WGS reaction (Reaction 2) to
14 favor more rapid H₂ production and CO consumption which simultaneously impedes the formation
15 of methane (Reactions 3 and 4).



19 The third and final step is the removal of CO₂ from the gaseous phase via carbon mineralization
20 using alkaline sorbents such as Ca- or Mg- hydroxides and alkaline industrial residues (e.g., Ladle
21 Slag generated during steel making) to produce stable solid carbonates with limited solubility in
22 water. The dissolution of Ca- or Mg-hydroxides or oxides mobilizes Ca²⁺ or Mg²⁺ ions which can
23 react with dissolved carbonates to produce solid Ca- or Mg-carbonates, as shown in Reactions 5-

1 9. The pH of our feedstock was found to increase from 4.88 – 7.67 to 12.25 – 12.29 post-addition
2 of Ca(OH)₂ and 12.15 – 12.19 post-addition of LD slag sorbent (See **Table S4**). Carbonate (CO₃²⁻
3) concentrations that are needed for carbon mineralization are favored over bicarbonate ions
4 (HCO₃⁻) with increase in pH (See **Figure S4**), which favors the formation of solid carbonates in
5 Reaction 8 – 9.

6 *Dissolution of Species*



10 *Carbonate Formation*



13 Despite the simplicity of the stoichiometric reactions describing the formation of Ca- or Mg-
14 carbonates, complex chemo-morphological interactions result in non-monotonic kinetics of
15 carbonate nucleation and growth. For example, the kinetics of carbon mineralization are strongly
16 influenced by the pH and composition of the aqueous phase,⁵¹ partial pressure of CO₂,⁵² and
17 temperature.³⁴ pH conditions greater than 8 favor (bi)carbonate formation which aid solid
18 carbonate formation while more acidic pH conditions favor the dissolution of Ca- or Mg-oxides
19 and hydroxides. Higher CO₂ partial pressures coupled with alkaline aqueous environments favor
20 CO₂ solvation and carbon mineralization.³⁶ Elevated temperatures favor dissolution of Ca- or Mg-
21 oxides and hydroxides and thermodynamically favor the precipitation of solid carbonates.³⁶ While
22 the thermodynamic feasibility of realizing CO₂ removal via carbon mineralization when coupled

1 with the deconstruction of biomass oxygenates has been established,²⁸ the associated kinetics have
2 not been discussed.

3 CO₂ removal via carbon mineralization can be integrated with the deconstruction of biomass
4 oxygenates in two modes. In the first mode, the aqueous biomass oxygenate, catalyst, and alkaline
5 sorbent are actively interacting in a slurry environment. In this mode, any evolved CO₂ can be
6 rapidly mineralized to produce solid carbonates when excess alkalinity is present. This approach,
7 if successful, can limit the ex-solution of CO₂ into the gas phase. However, carbonate formation
8 on the catalyst in the aqueous phase can lead to deactivation, after just one reaction. Alternatively,
9 another mode can be explored in which the alkaline sorbent can be placed in the gas phase. In this
10 mode, the deconstruction of biomass oxygenates in the aqueous phase results in the ex-solution of
11 CO₂ into the gas phase followed by mineralization. The mass transfer of CO₂ from the aqueous
12 phase to the gas phase, followed by the reactivity of CO₂ with the alkaline sorbent suspended in
13 the gas phase introduce additional “resistances” to *in-situ* CO₂ capture and removal. However, this
14 mode has the significant advantage that catalysts are not deactivated by solid carbonate formation,
15 and *in-situ* separation of solid carbonate products from the deconstructed aqueous biomass
16 oxygenate-bearing solutions and solid catalysts can be easily achieved. Thus, the experiments
17 conducted in this study and discussed in the followed sections, are designed to examine the
18 influence of these coupled multiphase chemical interactions on enhanced H₂ recovery with
19 inherent carbon removal, with the intent to inform appropriate reaction modes for scalable
20 deployment.

21 3.2 *Carbon removal effect on H₂ evolution during non-catalyzed hydrothermal treatment of*
22 *oxygenates*

1 Chemical reactions that proceed via cleavage of covalent bonds in organic compounds usually
2 have high activation energies. Hence, these pathways typically require a catalyst to lower their
3 activation energy for the reactions to occur fast enough over short time scales. In this study, a base
4 case scenario involving the hydrothermal conversion of 3 wt% methanol is conducted to elucidate
5 the effect of coupling mineralization reactions without a catalyst on the reforming process. In the
6 absence of a catalyst and an alkaline sorbent for *in-situ* CO₂ capture, H₂ yields obtained are less
7 than 1% after a reaction time of 3 hours (**Figure 3**). These low H₂ yields of < 1% are consistent
8 with the thermodynamic calculations reported in our prior studies.²⁸ However unlike predictions
9 from thermodynamic studies, hydrocarbons such as CH₄ are not detected in the gas product stream
10 for all cases studied in the absence of a catalyst. Results from product liquid analyses using NMR
11 in **Figure 3 (b)** show formate and acetate as the only intermediates formed when methanol is the
12 oxygenate precursor. From this observation and the absence of hydrocarbons in the product gas
13 stream, we infer that without a catalyst, H₂ production from methanol is likely to proceed solely
14 via the formation of formate as shown in **Figure 2 (b)**. In the formate pathway, methanol undergoes
15 partial oxidation to produce formate, which further produces CO₂ and H₂ via dehydrogenation.
16 Although no gaseous CO was observed in the product gas stream, we cannot completely rule out
17 the possibility of the formation of CO intermediates via the CO pathway. In the future, *operando*
18 measurements will be conducted to evaluate this hypothesis.

19 Over extended reaction residence time, we observed an increase in the concentration of acetate in
20 solution (**Figure 3 (b)**), which could be due to the recombination of CO₂, H₂ and methanol via
21 hydrocarboxylation to produce acetate.⁵³ The preferential formation of acetate through
22 hydrocarboxylation rather than methane formation via methanation is a very interesting
23 observation, especially since H₂ and CO₂ have been extensively reported to be thermodynamically

1 unstable compared to alkanes and water at low temperatures.⁴⁹ Overall, the kinetics of H₂ evolution
2 without a catalyst was observed to be greatly limited by biomass deconstruction to produce H₂ as
3 opposed to the formation of undesired products such as methane formation.

4 Further, we observed that H₂ and CO₂ yields increase, although very slowly with time (**Figures 3**
5 **(a), 3 (c) and 3 (d)**). In the presence of Ca(OH)₂ for CO₂ capture, a slight relative increase in H₂
6 yields in the range of 0.1 – 4.8% are achieved under similar conditions. While these results show
7 the importance of an alkaline environment in enhancing these reactions, it is also evident that
8 without a catalyst, these systems are severely limited by biomass deconstruction with or without
9 an alkaline sorbent. These results clearly demonstrate that catalysts are essential for biomass
10 oxygenate deconstruction, and their absence can severely limit H₂ evolution even when coupled
11 with exothermic carbon mineralization reactions.

12 3.3 *Effect of catalysts on enhanced H₂ yield without in-situ CO₂ removal*

13 High yield and selectivity for H₂ production from aqueous oxygenates is challenging to achieve
14 without an appropriate catalyst. To address this challenge, both Pt/Al₂O₃ and Ni/Al₂O₃ are selected
15 for this study given their effectiveness in reforming of heavy oxygenated hydrocarbons due to their
16 high activity for C-C cleavage.⁴⁹ Ni/Al₂O₃ catalyst shows better activity for both C-C breakage
17 and water gas shift reaction compared to Pt/Al₂O₃ catalysts,^{8,49,54} However, better catalyst
18 performance implies that the catalyst must also not facilitate undesired side reactions such as
19 methanation. **Figures 3 (c) & 3 (d)** show that H₂ yields of 20% are achieved in the presence of
20 Ni/Al₂O₃ catalysts with 3 wt% methanol after 1 hour of reaction time and at 240°C. Under similar
21 conditions, about 60 % H₂ yield was obtained using Pt/Al₂O₃. The lower H₂ yield obtained with
22 Ni/Al₂O₃ corresponds to the higher relative amount of methane produced. We observed that 25%

1 yield of methane was produced with Ni/Al₂O₃, whereas methane yields of < 1% were realized with
2 Pt/Al₂O₃ (**Figures 3 (c) & 3 (d)**). These observations of high H₂ selectivity with Pt/Al₂O₃ are
3 consistent with other studies reported in literature.⁵⁵ On this basis, Pt-based catalysts has been
4 consistently identified as a better catalyst for H₂ production. Regardless, the earth abundance, low
5 cost, and high biomass deconstruction activity provided by Ni-based catalysts are desirable for the
6 deconstruction of aqueous biomass oxygenates.

7 Longer reaction times of 6 hours increased CH₄ yield from methanol as the precursor as shown in
8 **Figures 3 (c) & 3 (d)**. An increase in CH₄ yield from 0.99% to 1.4 % is observed when the reaction
9 time increased from 1 hour to 6 hours in the presence of Pt/Al₂O₃ catalyst. The corresponding
10 increase in CH₄ yield in the presence of Ni/Al₂O₃ catalyst from 20.7% to 58% is more prominent.
11 A simultaneous decrease in H₂ yield observed in **Figures 3 (c) & 3 (d)** confirms that methane
12 formation occurs primarily due to gas phase selectivity reactions of CO/CO₂ favorable under these
13 conditions. Longer residence times imply more time for methane formation due to the increase in
14 CO₂ concentration. NMR analyses of the liquid products in **Figures S5-S7** in supporting
15 information confirm the presence of very low quantities of formate and acetate using either Pt or
16 Ni catalysts, thus supporting our earlier hypothesis that these reactions also proceed via the formate
17 formation route in **Figure 2 (b)**. These results also show that H₂ and CO₂ do recombine with
18 methanol via hydrocarboxylation to produce acetate. However, in the presence of a catalyst, H₂
19 and CO₂ recombine more selectively to produce methane in Reaction 4. Faster methanation on Ni
20 catalyst relative to that of Pt is consistent with the lower activity of Pt catalyst for methanation
21 reactions.

1 To obtain additional insights into the influence of catalyst morphology on reactivity, the pore sizes
2 and morphologies are determined using BET analyses. The specific surface area (SSA), pore
3 volume, and average pore diameter of the raw and spent Ni/Al₂O₃ and Pt/Al₂O₃ catalyst are
4 reported in **Table 2**. BET surface area of raw Ni/Al₂O₃ catalyst ($259.080 \pm 2.2\%$ m²/g) synthesized
5 in the lab are found to be higher than that of raw Pt/Al₂O₃ ($174.375 \pm 2.2\%$ m²/g). This observation
6 is attributed to the relatively smaller sizes of Al₂O₃ particles in the Ni/Al₂O₃ catalysts synthesized
7 in the lab. The number weighted average particle size of Ni/Al₂O₃ catalyst is 40 nm which is
8 considerably lower than that of Pt/Al₂O₃ which is 200 nm as shown in **Figure S8a** in the supporting
9 information section. Post-reaction, we observed a significant decrease in the surface area of
10 Ni/Al₂O₃ and Pt/Al₂O₃ catalysts. This is likely due to transformation of the catalyst & catalyst
11 support, in particular the hydration to Al₂O₃ to form boehmite was evident shown in **Figures S9**
12 **& S10** in the supporting information section. While the loading of Pt or Ni on Al₂O₃ support is the
13 same at 5 wt%, we do not eliminate the possibility that morphological features such as particle
14 size, pore size and surface area of a catalyst could potentially impact methane selectivity.
15 Formation of methane from aqueous phase reforming of butanol over Rh/ZrO₂ was recently found
16 to decrease from 0.25 mol CH₄/mol feedstock to 0.01 mol CH₄/mol feedstock as the catalyst
17 particle size increased from 40 - 60 μm to 250 - 420 μm, after 2 hours of reaction.²⁵ Lower
18 conversions of feedstocks were observed due to these morphological changes in the catalyst
19 particles. In contrast, an ideal scenario would be one where lower methane yields can be achieved
20 while maintaining high conversions of biomass oxygenates to desired gaseous products such as
21 H₂.

22 3.4 *Enhanced catalytically aided H₂ evolution with in-situ carbon removal*

1 While our work reported in the previous section, supported by extensive prior research,^{17,18,28,42,56}
2 have shown that catalysts are essential for deconstructing biomass oxygenates to produce CO₂ and
3 H₂, the hypothesis that *in-situ* CO₂ capture and removal will enhance H₂ yield (as shown in
4 Reaction 1) remains unexplored. To investigate the influence of alkaline sorbents, which is calcium
5 hydroxide (Ca(OH)₂) in this case, experiments are performed at temperatures of 240 °C and
6 pressures of 50 bar N₂ pressure using 3 wt% methanol solution. These results are summarized in
7 **Table S2** and **Figure 3**.

8 **Figure 3** shows that in the presence of Ca(OH)₂, methane yields are suppressed with either
9 Ni/Al₂O₃ or Pt/Al₂O₃ catalysts. CH₄ yields of about 6 % was obtained with Ni/Al₂O₃, when
10 Ca(OH)₂ is used for *in-situ* CO₂ capture which showed a significant decrease from ~ 58% obtained
11 without *in-situ* CO₂ capture after 6 hours of reaction. In contrast, CH₄ yield decreased from ~1.3%
12 to ~0.4% using Pt/Al₂O₃, with and without *in-situ* CO₂ capture. CO₂ removal via solid carbonate
13 formation leads to the depletion of CO₂ in the product stream and favors CO consumption as a
14 reactant which limits methane formation. Results showing CH₄ suppression using Pt/Al₂O₃ is not
15 as significant as results obtained with Ni/Al₂O₃ due to the relatively lower activity of Pt/Al₂O₃ to
16 methanation reactions shown in Reactions 3 & 4. Higher selectivity for H₂ with Pt/Al₂O₃ catalysts
17 is consistent with prior studies on biomass oxygenate deconstruction to produce H₂.⁴⁹ Interestingly,
18 H₂ yields as high as 74% are achieved in Mode II configuration in which Ca(OH)₂ is placed in the
19 gas phase, as opposed to 57% in Mode I configuration in which Ca(OH)₂ is in the aqueous phase,
20 for a reaction time of 6 hours using Ni/Al₂O₃ catalyst. Similarly, in the presence of Pt/Al₂O₃
21 catalyst, H₂ yields as high as 71% are achieved in Mode II configuration when Ca(OH)₂ is placed
22 in the gas phase, as opposed to 76% in Mode I configuration in which Ca(OH)₂ is in the aqueous
23 phase. Furthermore, longer reaction times up to 6 hours enhance H₂ yields in the presence of

1 Ni/Al₂O₃ catalyst and in Modes I and II. In contrast, increasing the reaction time from 3 to 6 hours
2 does not result in a significant enhancement in H₂ yield in Modes I and II in the presence of
3 Pt/Al₂O₃ catalyst. CO₂ concentrations in the product stream are negligible after reaction times of
4 3 hours and 6 hours when Ni/Al₂O₃ catalyst is used, and below 2% in the presence of Pt/Al₂O₃
5 catalyst.

6 These results are significant for several reasons. First, the effectiveness of Mode II in enhancing
7 H₂ yields with significant suppression of CO₂ yields is unexpected. It was hypothesized that the
8 direct contacting of the aqueous phase with Ca(OH)₂ promotes dissolution and rapid uptake of any
9 carbonate-bearing species without releasing CO₂ into the gas phase. In contrast, our results show
10 that gas-solid contacting of Ca(OH)₂ and CO₂ evolved during biomass oxygenate deconstruction
11 is also effective in enhancing H₂ yields with *in-situ* CO₂ capture. The low pH of the solution due
12 to the absence of an alkaline sorbent in the aqueous phase could be responsible for facilitating CO₂
13 ex-solution. **Figure S4** shows that the formation of H₂CO₃ (a precursor for CO₂ exsolution) is
14 more prominent at low pH. These results demonstrate that in-situ separation of the carbonate-
15 bearing product can be realized concurrently with enhanced H₂ yields. Interestingly, H₂ evolution
16 increases monotonically with time in Mode II unlike in Mode I in which higher reactivities are
17 achieved immediately due to the rapid uptake of CO₂ by calcium hydroxide in the aqueous phase.
18 In Mode II, *in-situ* CO₂ capture is the rate limiting step with higher longer reaction times
19 contributing to higher yields.

20 Further, H₂ evolution is observed to increase monotonically with time in mode II. This result also
21 makes sense as we had already established that the kinetics of biomass deconstruction reaction
22 proceeds at this time in cases without an alkaline sorbent. Also, if the reaction proceeds via the

1 CO pathway in **Figure 2 (b)**, the rapid increases of H₂ and CO₂ partial pressures coupled with the
2 relatively lesser void volume in mode II may also drive the reaction in the reverse direction at its
3 early stages to increase the CO concentration in the reactor, hence leading to lower rates due to
4 higher coverage of CO on the metal surface. Similar effects of CO on metal surface have been
5 reported.⁵⁷ Faster CO₂ capture rates are obtained with Mode I as shown in **Figures 4 (b) & 4 (d)**
6 which appears to be consistent with the faster kinetics observed with respect to H₂ yield in **Figure**
7 **3**. This fast kinetics in Mode I appeared to slow down significantly after 60 minutes of reaction,
8 which suggests that we could be experiencing mass transfer limitations likely due to the formation
9 of insoluble carbonates on active catalyst sites, preventing further H₂ production.

10 Progressive increases in calcium carbonate content observed in Modes I and II over Ni or Pt
11 catalysts shown in **Figures 4 (b) & 4 (d)** are consistent with observed calcium carbonate phases
12 in X-Ray Diffraction patterns in **Figure 4 (e)**. Stable calcite phases are formed as opposed to
13 metastable aragonite or vaterite phases, which is consistent with higher temperatures aiding the
14 formation of stable solid carbonate phases. The stability of the catalyst support is another
15 consideration during oxygenate reforming. From XRD plots in **Figure 4 (e) and Figure S10 (b)**,
16 we observed the conversion of alumina (Al₂O₃) support to a less active crystalline boehmite
17 (AlOOH) phase. The presence of acetate has been reported to be responsible for the deactivation
18 of Pt & Ni on alumina catalysts by hydroxylation of the Al₂O₃ surface, which forms crystalline
19 boehmite (AlOOH) and leads to catalyst deactivation.^{20,58} The observations from XRD analyses
20 are supported by evidence of bonding behavior of, Al-O vibrations from FTIR spectra in **Figure**
21 **4 (f) and Figure S10 (a)**. *In-situ* separation of the spent catalyst and solid carbonate product with
22 Mode II can also be observed by the bonding behavior of, C-O, C=O and O-H vibrations from
23 FTIR spectra in **Figure 4 (f)**. Further evidence of the conversion of calcium hydroxide to calcium

1 carbonate and the absence of boehmite (AlOOH) phase in Mode II unlike Mode I is confirmed
2 from Thermogravimetric Analysis (TGA) in **Figures 4 (a) & 4 (c)**. In Mode I with either $\text{Ni}/\text{Al}_2\text{O}_3$
3 or $\text{Pt}/\text{Al}_2\text{O}_3$ catalyst and calcium hydroxide in the aqueous phase, three distinct weight loss regimes
4 are noted in the range of $360^\circ\text{C} - 430^\circ\text{C}$, $440^\circ\text{C} - 540^\circ\text{C}$, and $550^\circ\text{C} - 800^\circ\text{C}$, which correspond to
5 the dehydration of $\text{Ca}(\text{OH})_2$, dehydration of AlOOH , and the dissociation of CaCO_3 , respectively.
6 In contrast, dehydration of $\text{Ca}(\text{OH})_2$ and the dissociation of CaCO_3 are noted in Mode II. Further,
7 DSC curves confirms an endothermic profile associated with the weight losses observed in DTG
8 curves.

9 *3.5 Enhanced H_2 production with in-situ carbon removal using heavier aqueous oxygenates*

10 Feedstock variability and associated uncertainty in mechanisms and kinetics have been challenges
11 in adapting innovative routes for producing H_2 from biomass feedstocks with inherent carbon
12 removal.⁵⁹ To address this challenge, we investigate the influence of heavier $\text{C}_1\text{-C}_3$ oxygenated
13 hydrocarbons such as glycerol, ethylene glycol, acetate, and formate on enhancing H_2 yields with
14 and without inherent carbon removal. These oxygenates were chosen because they can be readily
15 obtained in large quantities from low value biomass feedstocks such as food or municipal waste
16 generated in urban or rural environments, algal sources, and industrial wastewater polluted
17 streams.²⁸ Experiments were conducted over $\text{Pt}/\text{Al}_2\text{O}_3$ and $\text{Ni}/\text{Al}_2\text{O}_3$ catalyst at 240°C , and 50 bar
18 N_2 pressure. Experiments are performed in Mode II since it has been shown that high H_2 yields,
19 and selectivity are achieved with in-situ separation of CO_2 as solid carbonate and ease of catalyst
20 recovery. Varying the feedstock has been shown to have a strong influence on H_2 selectivity due
21 to differing deconstruction mechanisms. It has been reported that within the family of polyols, the
22 hydrogen selectivity of aqueous phase reforming decreases with increasing carbon number of the

1 feed.⁴⁹ Therefore, the influence of these differing deconstruction mechanisms on H₂ yields with
2 and without CO₂ removal from aqueous biomass oxygenates are investigated. Yields of H₂, CO₂,
3 CH₄, CO, and CaCO₃ are shown in **Figure 5** and summarized in **Table S2**.

4 In the absence of *in-situ* CO₂ removal, H₂ yields of ~ 15%, 19%, 2%, and 45% are achieved in the
5 presence of Ni/Al₂O₃ catalyst and ~ 49%, 79%, 3%, and 71% in the presence of Pt/Al₂O₃ catalyst
6 for glycerol, ethylene glycol, acetate, and formate respectively. In contrast, H₂ yields when coupled
7 to *in-situ* CO₂ removal are ~ 73%, 90%, 8%, and 65% in the presence of Ni/Al₂O₃ catalyst and ~
8 69%, 85%, 9%, and 73% in the presence of Pt/Al₂O₃ catalyst for glycerol, ethylene glycol, acetate,
9 and formate respectively. Without *in-situ* CO₂ capture, higher H₂ yields are consistently achieved
10 with formate using either Ni/Al₂O₃ or Pt/Al₂O₃ catalyst since H₂ production proceeds directly
11 through the formate dehydrogenation pathway to produce H₂ and CO₂ as shown in **Figure 2 (b)**.
12 High H₂ yields are also accompanied by relatively lower methane yields ~0.2% and 4.5% with
13 Ni/Al₂O₃ and Pt/Al₂O₃ respectively using formate as the starting feedstock. This is likely due to
14 the elimination of possible methane formation via CO methanation in Reaction 3, Further, the
15 formation of water-soluble sodium bicarbonate species from the interaction of bicarbonate and
16 sodium ions in solution as shown in **Table S1** prevents CO₂ production, and subsequently CO₂
17 methanation which results in low yields of CO₂ and CH₄ (**Figure 5 (b)**). It is also interesting to
18 note that formate is observed to be an intermediate liquid precursor using all oxygenates studied
19 as starting feedstock. This was confirmed by NMR analyses on liquid products obtained post-
20 reaction shown in **Figure S7** .

21 In contrast, lowest H₂ yields are achieved with acetate as the starting feedstock for several reasons.
22 First, we can observe that either C-C or C-O bond cleavage of acetate results in the preferential
23 formation of CH₄ prior to CO or CO₂ formation, which limits H₂ production (**Figure 2 (b)**).

1 Second, the possibility of regenerating acetate via hydrocarboxylation also exists, which further
2 leads to H₂ consumption.⁵³ Acetate has also been reported to be responsible for the deactivation of
3 Pt–Ni catalysts by hydroxylation of the Al₂O₃ surface.⁶⁰ Subsequent re-deposition of the dissolved
4 alumina on the catalyst causes blocking of active catalytic Ni/Pt sites which leads to catalyst
5 deactivation and hence limits feedstock conversion.⁹ These results show that either biomass
6 deconstruction or acetate regeneration could be limiting H₂ evolution and represents an interesting
7 selectivity challenge that requires further investigation in our future work. H₂ yields of 20 – 80 %
8 are also noted with ethylene glycol and glycerol without *in-situ* CO₂ capture, although more
9 methane formation was observed with glycerol. This is most likely due to the higher possibility of
10 methane formation via C-O cleavage with glycerol relative to ethylene glycol, due to the presence
11 of more O-H bonding sites for C-O cleavage in glycerol. Just as in the case of methanol, **Figure 5**
12 also shows considerable methane suppression with *in-situ* CO₂ removal with all biomass
13 oxygenates except for acetate. Unsurprisingly, lower H₂ yields with acetate were observed even
14 after coupling mineralization reactions in the presence of platinum and nickel catalysts. From
15 results shown in **Figure 5**, we can infer that the selectivity for H₂ production improves in the order
16 acetate < glycerol < ethylene glycol ~ methanol < formate without *in-situ* CO₂ capture and acetate
17 < glycerol < methanol < formate < ethylene glycol with *in-situ* CO₂ capture using Ni and Pt on
18 alumina catalyst. This trend was similar with experimental results obtained via aqueous phase
19 reforming by Davda and co-workers⁴⁹ who reported that the order of biomass oxygenate reactivity
20 is as follows: glucose < sorbitol < glycerol < ethylene glycol < methanol.

21 3.6 *Model waste stream upcycling with carbon mineralization using alkaline rich industrial*
22 *residues*

1 To probe the enhancement in hydrogen production from oxygenates using alkaline industrial
2 residues, ladle slag was used as an alkaline sorbent in the presence of Ni/Al₂O₃ catalysts. Model
3 wastewater was also prepared in lab using 3 wt.% of a mixture of formate, acetate, glycerol,
4 ethylene glycol and methanol to show the applicability of this process with heterogenous streams.
5 H₂ yields of 58% and 19% yield are observed with and without ladle slag, respectively. Further,
6 methane suppression is also noted as methane yields are reduced from 29 % and 6% in the presence
7 of ladle slag as an alkaline sorbent. We also detected an increase in the solid Ca- and Mg-carbonate
8 content resulting from the capture and conversion of 70% of CO₂ released from the deconstruction
9 of biomass oxygenates.

10 The solid product collected post-reaction is characterized by X-Ray Diffraction (XRD), as shown
11 in **Figure 6 (b)**. The main crystalline phases of fresh ladle slag are Ca(OH)₂ (portlandite), SiO₂
12 (Silica), Mg(OH)₂ (brucite), and MgO (magnesia). Post reaction, a significant increase of peak
13 intensities for CaCO₃ (calcite), and the appearance of phases such as Mg₂CO₃(OH)₂.3H₂O (artinite)
14 is observed. while peak intensities corresponding to both, Ca(OH)₂ and MgO are significantly
15 reduced. These results agree with the FTIR spectra analyses. Doublet O-H peaks at 3580 – 3650
16 and 3650 – 3720 cm⁻¹ are observed in the FTIR spectra of freshly milled ladle slag in **Figure 6 (d)**
17 which corresponds to the vibrations from Ca(OH)₂, and Mg(OH)₂ respectively, Si-O vibrations are
18 also observed at 900 – 1000 cm⁻¹. The asymmetric stretching vibration band of C-O at 1420 – 1480
19 cm⁻¹ bands and the bending vibrations of CO₃²⁻ peaks at 873 and 712 cm⁻¹ are prominent in the
20 carbonate product. Post reaction, we observe a decrease in the intensity of Ca(OH)₂ and an increase
21 in the intensity of Mg(OH)₂. This increase in O-H intensity associated with Mg(OH)₂ is due to
22 both the synthesis of Mg(OH)₂ via the reaction of MgO with water, and the simultaneous formation
23 of Mg₂CO₃(OH)₂.3H₂O via carbon mineralization of Mg(OH)₂. Further evidence of carbon

1 mineralization are observed with TGA plots in **Figures 6 (a) and 6 (c)**, which shows four distinct
2 weight loss corresponding to $\text{Mg}(\text{OH})_2$, $\text{Ca}(\text{OH})_2$, MgCO_3 , and CaCO_3 respectively. These results
3 conclusively demonstrate that the Ca- and Mg-bearing phases in Ladle Slag are the main reacting
4 components with CO_2 to form the carbonate minerals, as shown by Reactions 8 – 12.

5 **4. Conclusion**

6 This study has shown that high purity H_2 can be produced with inherent CO_2 removal from various
7 biomass oxygenate sources including methanol, glycerol, ethylene glycol, acetate, and formate
8 using alkaline industrial residues (Ladle Slag) as Ca- & Mg- bearing sources. As opposed to
9 conventional high temperature reforming processes ($>500\text{ }^\circ\text{C}$) at atmospheric pressure, we
10 investigated the effect of maintaining fluids in the aqueous phase under N_2 pressure of 50 bar and
11 at significantly lower temperature of $240\text{ }^\circ\text{C}$. Coupling aqueous phase biomass oxygenate
12 reforming with thermodynamically downhill carbon mineralization reactions for *in-situ* CO_2
13 capture successfully enhanced H_2 production. For example, $\sim 90\%$ vs $\sim 19\%$ H_2 yield was obtained
14 with and without *in-situ* CO_2 capture respectively using ethylene glycol as starting feedstock, over
15 $\text{Ni}/\text{Al}_2\text{O}_3$ catalyst. Further, methane formation has been a long-standing challenge with Ni based
16 catalysts. Our study also showed suppressed methanation rates ($\sim 4\%$ vs 30% CH_4 yield) with and
17 without *in-situ* CO_2 capture respectively using ethylene glycol as starting feedstock, over $\text{Ni}/\text{Al}_2\text{O}_3$
18 catalyst. H_2 evolution is also studied using two modes of operations. While Mode I which favors
19 the formation of carbonate species in solution showed faster kinetics, *in-situ* product separation is
20 also shown to be achievable via Mode II in which mineralization proceeds after CO_2 ex-solution.
21 H_2 yields as high as 79% and 74% are achieved using ethylene glycol and methanol in the presence
22 of Ni or $\text{Pt}/\text{Al}_2\text{O}_3$ catalyst and $\text{Ca}(\text{OH})_2$ as the alkaline sorbent. Approximately 53% H_2 yield was
23 obtained from model $\text{C}_1 - \text{C}_3$ carbon bearing wastewater stream using ladle slag as the alkaline

1 sorbent, with over 70% of CO₂ released from the deconstruction of biomass oxygenates captured
2 and converted as solid Ca- or Mg-carbonates. This study provides a novel pathway in which large
3 amounts of low value residues such as Ca-rich alkaline residues and wastewater streams bearing
4 biomass oxygenates can be successfully upcycled to produce high value H₂ with inherent CO₂
5 removal.

6 **Authors' contributions**

7 Conceptualization: G.G., and P.O.; Data curation: G.G., and P.O.; Formal Analysis: G.G., P.O.,
8 S.M., A.M., and C.N.; Funding acquisition: G.G. and P.O.; Methodology: G.G. and P.O.; Project
9 administration: G.G.; Resources: G.G., P.O.; Supervision: G.G.; Visualization: G.G., P.O., S.M.,
10 A.M., C.N.; Writing – original draft: G.G., and P.O.; Writing – review & editing: G.G., P.O., S.M.,
11 A.M., C.N.; contributed equally to this work. All authors contributed to the discussion and
12 provided feedback on the manuscript.

13 **Conflicts of interest**

14 There are no conflicts to declare.

15 **Acknowledgment**

16 The authors also acknowledge the use of the shared facilities at the Cornell Center for Materials
17 Research (CCMR) which are supported through the National Science Foundation Materials
18 Research Science and Engineering Centers (NSF MRSEC) program (DMR-1719875). G. G.'s
19 contributions are supported by the DOE CAREER Award through the Office of Science DE-
20 658308. P. O.'s efforts are supported by the Cornell Atkinson Small Grant Program through the
21 Reducing Climate Risk initiative funded by the Cornell Atkinson Center for Sustainability, Cornell
22 University, and the Link Foundation Energy Fellowship. C. N.'s effort was supported by the

1 Cornell University Luis Stokes Alliance for Minority Participation (LSAMP) Program. We would
2 also like to thank Ivan Keresztes, current director for the NMR facility at the Department of
3 Chemistry and Chemical Biology, Cornell University for supporting our NMR experiments and
4 analyses. Finally, we would like to thank Cord Heine, the environmental supervisor at Nucor Inc.,
5 in Auburn, NY for providing us with industrial residues used for this study.

6 **References**

- 7 1 S. J. Davis, N. S. Lewis, M. Shaner, S. Aggarwal, D. Arent, I. L. Azevedo, S. M. Benson,
8 T. Bradley, J. Brouwer, Y. M. Chiang, C. T. M. Clack, A. Cohen, S. Doig, J. Edmonds, P.
9 Fennell, C. B. Field, B. Hannegan, B. M. Hodge, M. I. Hoffert, E. Ingersoll, P. Jaramillo,
10 K. S. Lackner, K. J. Mach, M. Mastrandrea, J. Ogden, P. F. Peterson, D. L. Sanchez, D.
11 Sperling, J. Stagner, J. E. Trancik, C. J. Yang and K. Caldeira, *Science* (80-.), ,
12 DOI:10.1126/science.aas9793.
- 13 2 M. A. R. S. Koohi-fayegh, *Energy, Ecol. Environ.*, 2016, **1**, 10–29.
- 14 3 M. A. Pellow, C. J. M. Emmott, C. J. Barnhart and S. M. Benson, *Energy Environ. Sci.*,
15 2015, **8**, 1938–1952.
- 16 4 L. Chen, Z. Qi, S. Zhang, J. Su and G. A. Somorjai, *Catalysts*, ,
17 DOI:10.3390/catal10080858.
- 18 5 B. Parkinson, P. Balcombe, J. F. Speirs, A. D. Hawkes and K. Hellgardt, *Energy Environ.*
19 *Sci.*, 2019, **12**, 19–40.
- 20 6 F. Eljack and M.-K. Kazi, *Front. Sustain.*, 2021, **1**, 1–15.
- 21 7 S. Zhang, Y. Liu, M. Zhang, Y. Ma, J. Hu and Y. Qu, *Nat. Commun.*, ,

- 1 DOI:10.1038/s41467-022-33186-z.
- 2 8 P. D. Vaidya and J. A. Lopez-Sanchez, *ChemistrySelect*, 2017, **2**, 6563–6576.
- 3 9 T. M. C. Hoang, A. K. K. Vikla and K. Seshan, *Aqueous-phase reforming of sugar*
4 *derivatives: Challenges and opportunities*, 2016, vol. 2016- Janua.
- 5 10 A. I. Osman, N. Mehta, A. M. Elgarahy, M. Hefny, A. Al-Hinai, A. H. Al-Muhtaseb and
6 D. W. Rooney, *Hydrogen production, storage, utilisation and environmental impacts: a*
7 *review*, Springer International Publishing, 2022, vol. 20.
- 8 11 G. Zoppi, G. Pipitone, R. Pirone and S. Bensaid, *Catal. Today*, 2022, **387**, 224–236.
- 9 12 J. Plácido and S. Capareda, *Bioresour. Bioprocess.*, 2016, **3**, 1–12.
- 10 13 U.S. Energy Information Administration, *Monthly Biodiesel Production Report*, 2015.
- 11 14 F. Yang, M. A. Hanna and R. Sun, *Biotechnol. Biofuels*, 2012, **5**, 1–10.
- 12 15 J. Moestedt, B. Müller, Y. Nagavara Nagaraj and A. Schnürer, *Front. Energy Res.*, 2020,
13 **8**, 1–15.
- 14 16 T. Uekert, F. Dorchies, C. M. Pichler and E. Reisner, *Green Chem.*, 2020, **22**, 3262–3271.
- 15 17 I. Coronado, M. Stekrova, L. García Moreno, M. Reinikainen, P. Simell, R. Karinen and J.
16 Lehtonen, *Biomass and Bioenergy*, 2017, **106**, 29–37.
- 17 18 Z. Xiong, Z. Fang, L. Jiang, H. Han, L. He, K. Xu, J. Xu, S. Su, S. Hu, Y. Wang and J.
18 Xiang, *Fuel*, 2022, **314**, 122746.
- 19 19 L. André, S. Abanades and G. Flamant, *Renew. Sustain. Energy Rev.*, 2016, **64**, 703–715.
- 20 20 D. A. Boga, F. Liu, P. C. A. Bruijninx and B. M. Weckhuysen, *Catal. Sci. Technol.*,

- 1 2016, **6**, 134–143.
- 2 21 R. R. Davda and J. A. Dumesic, *Chem. Commun.*, 2004, **4**, 36–37.
- 3 22 M. Alvear, A. Aho, I. L. Simakova, H. Grénman, T. Salmi and D. Y. Murzin, *Catal. Sci.*
4 *Technol.*, 2020, **10**, 5245–5255.
- 5 23 H. Xiong, A. DeLaRiva, Y. Wang and A. K. Datye, *Catal. Sci. Technol.*, 2015, **5**, 254–
6 263.
- 7 24 T. Nozawa, Y. Mizukoshi, A. Yoshida and S. Naito, *Applied Catal. B, Environ.*, 2014,
8 **146**, 221–226.
- 9 25 H. Harju, G. Pipitone and L. Lefferts, *Front. Chem.*, 2020, **8**, 1–13.
- 10 26 J. Zhang, W. Yan, Z. An, H. Song and J. He, *ACS Sustain. Chem. Eng.*, 2018, **6**, 7313–
11 7324.
- 12 27 S. Jeon, H. S. Roh, D. J. Moon and J. W. Bae, *RSC Adv.*, 2016, **6**, 68433–68444.
- 13 28 P. Ochonma, C. Blaudeau, R. Krasnoff and G. Gadikota, *Front. Energy Res.*, 2021, **9**, 1–
14 16.
- 15 29 F. Raganati, F. Miccio and P. Ammendola, *Energy and Fuels*, 2021, **35**, 12845–12868.
- 16 30 T. Yin, S. Yin, A. Srivastava and G. Gadikota, *Resour. Conserv. Recycl.*, 2022, **180**,
17 106209.
- 18 31 S. Fujikawa, R. Selyanchyn and T. Kunitake, *Polym. J.*, 2021, **53**, 111–119.
- 19 32 S. Kodama, T. Nishimoto, N. Yamamoto, K. Yogo and K. Yamada, *Energy*, 2008, **33**,
20 776–784.

- 1 33 G. Gadikota, *Commun. Chem.*, 2021, **4**, 1–5.
- 2 34 M. Liu and G. Gadikota, *Fuel*, 2020, **275**, 1–37.
- 3 35 G. Gadikota, *Nat. Rev. Chem.*, 2020, **4**, 78–89.
- 4 36 G. Gadikota, J. Matter, P. Kelemen and A. H. A. Park, *Phys. Chem. Chem. Phys.*, 2014,
5 **16**, 4679–4693.
- 6 37 V. Nikulshina, M. E. Gálvez and A. Steinfeld, *Chem. Eng. J.*, 2007, **129**, 75–83.
- 7 38 A. Stefánsson, P. Bénézeth and J. Schott, *Geochim. Cosmochim. Acta*, 2014, **138**, 21–31.
- 8 39 T. N. Borhani and M. Wang, *Renew. Sustain. Energy Rev.*, 2019, **114**, 109299.
- 9 40 J. W. Shabaker, G. W. Huber and J. A. Dumesic, *J. Catal.*, 2004, **222**, 180–191.
- 10 41 B. Roy and C. A. Leclerc, *J. Power Sources*, 2015, **299**, 114–124.
- 11 42 R. L. Manfro, T. P. M. D. Pires, N. F. P. Ribeiro and M. M. V. M. Souza, *Catal. Sci.*
12 *Technol.*, 2013, **3**, 1278–1287.
- 13 43 R. Ragipani, S. Bhattacharya and A. K. Suresh, *React. Chem. Eng.*, 2021, **6**, 1152–1178.
- 14 44 B. Xu and Y. Yi, *Chemosphere*, , DOI:10.1016/j.chemosphere.2021.132274.
- 15 45 G. Gadikota and A. hyung A. Park, *Accelerated Carbonation of Ca- and Mg-Bearing*
16 *Minerals and Industrial Wastes Using CO₂*, Elsevier B.V., 2015.
- 17 46 S. Y. Pan, T. C. Chung, C. C. Ho, C. J. Hou, Y. H. Chen and P. C. Chiang, *Sci. Rep.*,
18 2017, **7**, 1–11.
- 19 47 M. Fridahl and M. Lehtveer, *Energy Res. Soc. Sci.*, 2018, **42**, 155–165.

- 1 48 J. Rogelj, D. Shindell, K. Jiang, S. Fifita, P. Forster, V. Ginzburg, C. Handa, H. Kheshgi,
2 S. Kobayashi and E. Kriegler, *Glob. Warm. 1.5° C*, 2018, 93–174.
- 3 49 R. R. Davda, J. W. Shabaker, G. W. Huber, R. D. Cortright and J. A. Dumesic, *Appl.*
4 *Catal. B Environ.*, 2005, **56**, 171–186.
- 5 50 J. De Heer, *J. Chem. Educ.*, 1957, **34**, 375–380.
- 6 51 A. Korchef and M. Touaibi, *Water Environ. J.*, 2020, **34**, 331–341.
- 7 52 G. Gravogl, F. Birkelbach, D. Müller, C. L. Lengauer, P. Weinberger and R. Miletich,
8 *Adv. Sustain. Syst.*, 2021, **5**, 1–11.
- 9 53 Q. Qian, J. Zhang, M. Cui and B. Han, *Nat. Commun.*, 2016, **7**, 1–7.
- 10 54 D. Li, Y. Li, X. Liu, Y. Guo, C. W. Pao, J. L. Chen, Y. Hu and Y. Wang, *ACS Catal.*,
11 2019, **9**, 9671–9682.
- 12 55 N. D. Subramanian, J. Callison, C. R. A. Catlow, P. P. Wells and N. Dimitratos, *Int. J.*
13 *Hydrogen Energy*, 2016, **41**, 18441–18450.
- 14 56 G. Pipitone, G. Zoppi, R. Pirone and S. Bensaid, *Int. J. Hydrogen Energy*, 2022, **47**, 151–
15 180.
- 16 57 A. Patra, H. Peng, J. Sun and J. P. Perdew, *Phys. Rev. B*, 2019, **100**, 1–8.
- 17 58 C. Liu, K. Shih, Y. Gao, F. Li and L. Wei, *J. Soils Sediments*, 2012, **12**, 724–733.
- 18 59 J. Feroso, L. He and D. Chen, *J. Chem. Technol. Biotechnol.*, 2012, **87**, 1367–1374.
- 19 60 D. J. M. De Vlieger, B. L. Mojet, L. Lefferts and K. Seshan, *J. Catal.*, 2012, **292**, 239–
20 245.

1

2

3

4

5

6

7

8

9

10

11

12

13

14

15

16

17

18 **Table 1.** Major elemental compositions of ladle slag (wt. %) using X-ray fluorescence analyses (XRF).

19 Ladle slag is a by-product of Nucor's electric arc furnace steel making process.

Compositions (%)	Nucor Electric Arc Furnace Ladle Slag
SiO ₂	9.66
Al ₂ O ₃	11.20
Fe ₂ O ₃	5.35
MgO	31.30
CaO	33.40
Na ₂ O	0.08
K ₂ O	0.10
TiO ₂	0.51
P ₂ O ₅	0.09
MnO	0.92
Cr ₂ O ₃	0.11
V ₂ O ₅	0.02
LOI	6.40
C (t)	0.34
S	0.14

1

2

3

4

5

6

7

8

9 **Table 2.** Surface area, pore size volume, and average pore diameter of the materials in this study.

Samples	Surface Area ^a	Pore size volume ^b	Average Pore
	(m ² /g)	(cc/g)	Diameter ^c (nm)
Alkaline Feedstock(Ca(OH) ₂)	31.35	0.13	3.85
Raw Catalyst (Ni)	259.08	0.42	6.30
Raw Catalyst (Pt)	174.37	0.28	5.83
Catalyst (Ni) + Ca(OH) ₂	174.18	0.30	6.29
Catalyst (Pt) + Ca(OH) ₂	112.94	0.20	5.83
Product (CaCO ₃)	8.38	0.02	2.75
Used Catalyst (Ni)	30.53	0.10	3.92
Used Catalyst (Pt)	15.69	0.10	3.07
Used Catalyst (Ni) + Product (CaCO ₃)	10.83	0.07	4.00
Used Catalyst (Pt) + Product (CaCO ₃)	9.18	0.04	2.99
Ladle Slag	9.18	0.03	3.84
Ladle Slag after reaction	38.41	0.08	3.85

1
2 ^aCalculated using the BET equation. ^bBJH pore desorption volume. ^cDesorption average pore
3 diameter.

4 Measurements are reported within BET error range of $\pm 2.2\%$

5

6

7 Captions for Figures

8 **Figure 1.** Schematic representation of integrated H₂ production from aqueous biomass oxygenates
9 with in-situ CO₂ capture using alkaline industrial residues.

10 **Figure 2.** (a) Reaction configurations for H₂ evolution with in-situ CO₂ capture and mineralization.
11 In Mode I, the catalyst, alkaline sorbent, and oxygenate feedstock are mixed to form a slurry. In
12 Mode II, the alkaline sorbent is suspended in the gas phase, while the catalyst and feedstock are

1 mixed in the liquid phase. (b) Reaction pathways associated with the deconstruction of oxygenates
2 to produce H₂ from aqueous biomass oxygenates are shown.

3 **Figure 3.** (a) Gas product yield for base case (without a catalyst) H₂ production from the
4 hydrothermal treatment of 3 wt.% methanol with and without an alkaline sorbent (Ca(OH)₂). (b)
5 H₂O Suppressed NMR spectra of liquid products from temporal evolution resulting from the
6 deconstruction of oxygenates in the presence of alkaline sorbents in contact with fluid phase (Mode
7 I). Only the dominant vibrations are labeled, and the spectra are offset for clarity. (c) Product yields
8 in the gas phase when Ni/Al₂O₃ catalyst is used during the hydrothermal treatment of 3 wt.%
9 methanol with and without an alkaline sorbent (Ca(OH)₂) (d) Product yields in the gas phase when
10 Pt/Al₂O₃ catalyst is used during the hydrothermal treatment of 3 wt.% methanol with and without
11 an alkaline sorbent (Ca(OH)₂). Alkaline sorbent reactions are carried out in Mode I (catalyst,
12 sorbent and feedstock are mixed to form a slurry), and Mode II (sorbent is suspended in the gas
13 phase, while the catalyst and feedstock are mixed in the liquid phase), at temperatures of 240 °C
14 and pressures of 50 bar N₂ pressure.
15 NA: No Alkalinity, NC: No Catalyst, M1: Mode I, and M2: Mode II.

16 **Figure 4.** Evidence of calcium carbonate formation in the solid product obtained from H₂
17 production via hydrothermal treatment of 3 wt.% methanol based on: (a) thermo gravimetric
18 analysis of solid calcium carbonate product from Mode I, (b) calculated extent of calcium
19 carbonate formation in solid product obtained from Mode I, (c) thermo gravimetric analysis of
20 solid product from Mode II, (d) calculated extent of calcium carbonate formation in solid product
21 obtained from Mode I, (e) XRD analyses showing calcium carbonate phases formed post-reaction,
22 and (f) FTIR analyses of solid calcium carbonate products obtained post-reaction.

23 **Figure 5.** Yields of H₂, CO₂, CH₄, CO, and CaCO₃ resulting from the hydrothermal conversion of
24 3 wt.% biomass oxygenates to H₂ with inherent carbon removal using Ca(OH)₂ sorbent where (a),
25 (b), (c), and (d) represent glycerol, formate, acetate, and ethylene glycol, respectively. NA
26 represents the scenario when there is no alkalinity in the system. M2 represents Mode II in which
27 the alkaline sorbent is suspended in the gas phase, the catalyst and feedstock are mixed in the liquid
28 phase, and the reaction temperature and N₂ pressure are 240°C and 50 bar, respectively.

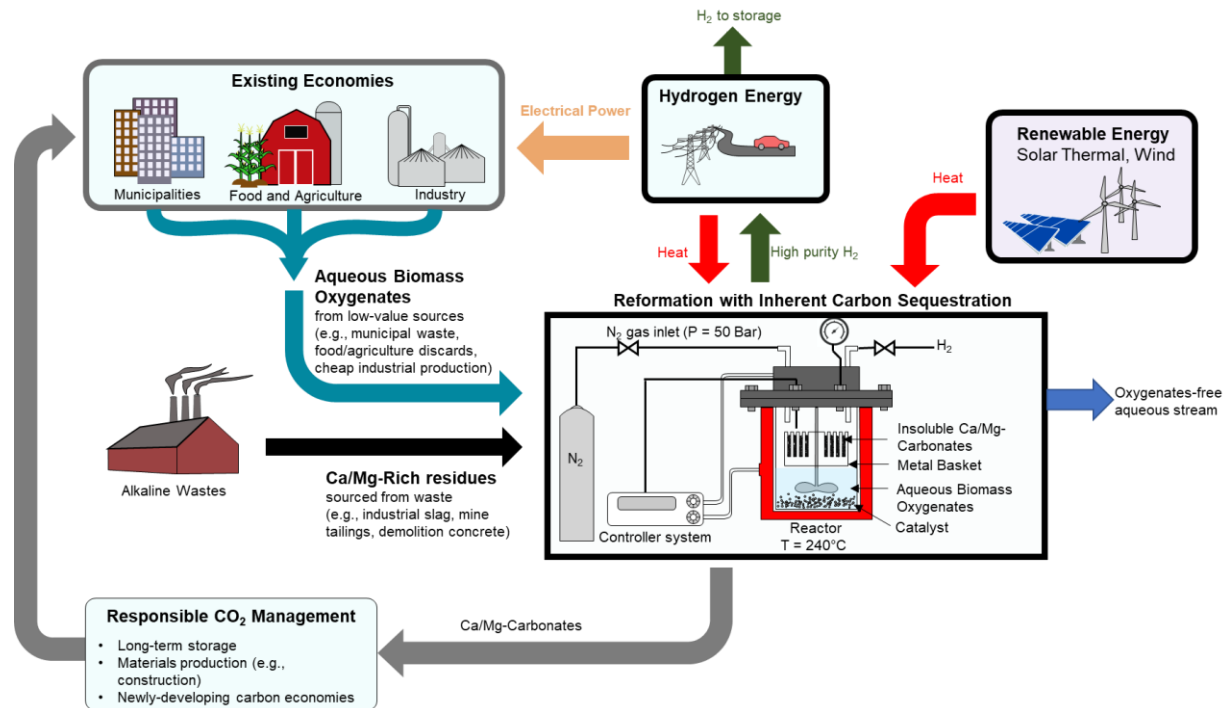
29 **Figure 6.** Contrasting unreacted and reacted ladle slag obtained after H₂ conversion from model
30 wastewater and CO₂ removal from ladle slag with *in-situ* CO₂ capture using (a) DSC
31 measurements, (b) XRD analyses, (c) DTG curves, (d) FTIR analyses, (e) product yields on using
32 Ni/Al₂O₃ catalyst, and (f) H₂O suppressed NMR spectra of liquid products. Only the dominant
33 vibrations are labeled, and the spectra are offset for clarity in (f). Reactions are carried out in Mode
34 II where the sorbent is suspended in the gas phase, while Ni/Al₂O₃ catalyst and mixture of biomass
35 oxygenates are mixed in the liquid phase, at temperatures of 240 °C and N₂ pressure of 50 bar.

36

37

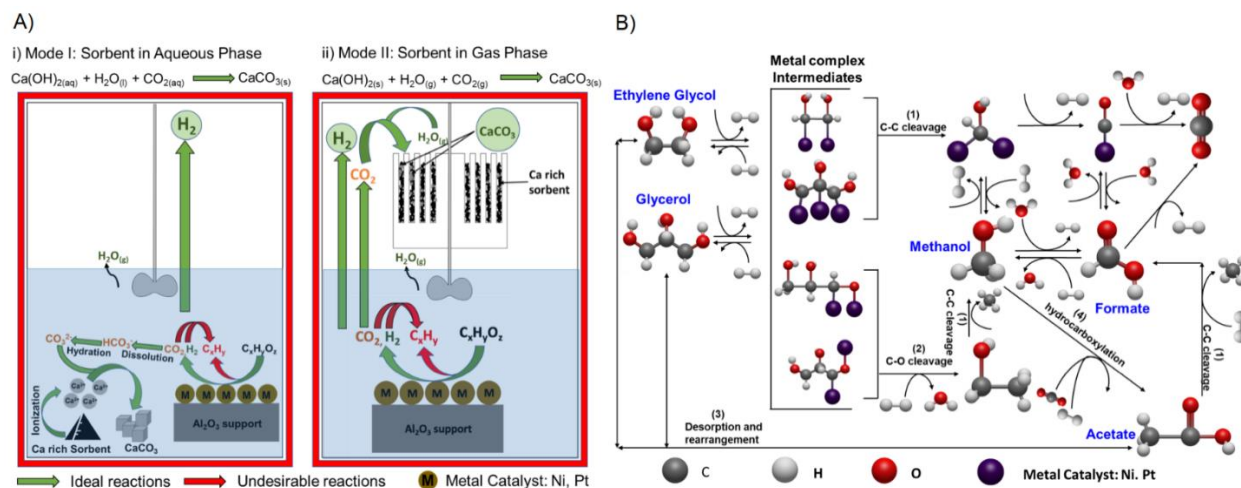
38

- 1
- 2
- 3
- 4
- 5
- 6
- 7
- 8
- 9
- 10
- 11
- 12
- 13
- 14
- 15
- 16
- 17
- 18
- 19
- 20
- 21
- 22



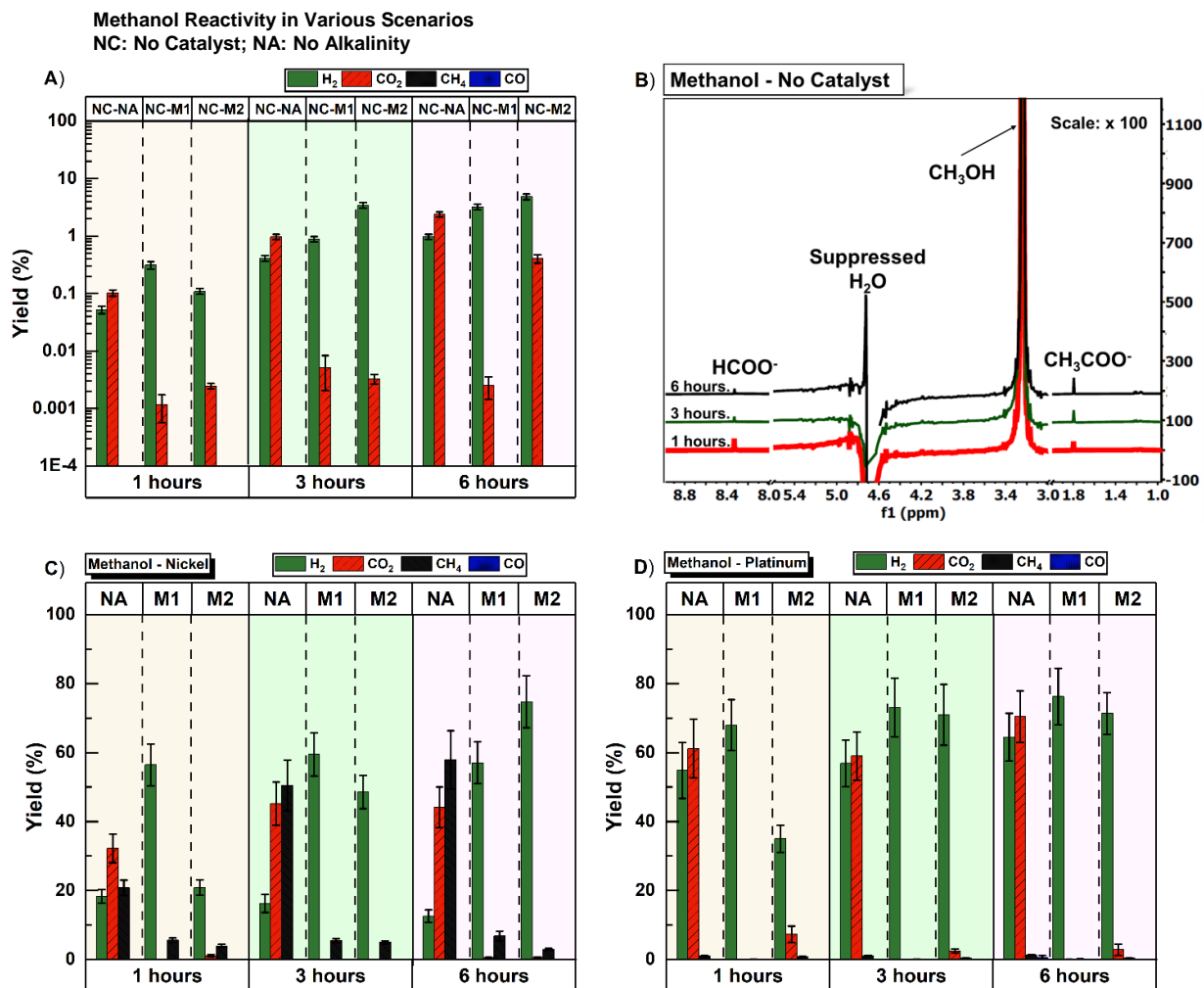
1
2
3
4
5
6
7
8
9
10
11
12
13
14
15

Figure 1. Schematic representation of integrated H_2 production from aqueous biomass oxygenates with in-situ CO_2 capture using alkaline industrial residues.



1
 2 **Figure 2.** (a) Reaction configurations for H_2 evolution with in-situ CO_2 capture and mineralization.
 3 In Mode I, the catalyst, alkaline sorbent, and oxygenate feedstock are mixed to form a slurry. In
 4 Mode II, the alkaline sorbent is suspended in the gas phase, while the catalyst and feedstock are
 5 mixed in the liquid phase. (b) Reaction pathways associated with the deconstruction of oxygenates
 6 to produce H_2 from aqueous biomass oxygenates are shown.

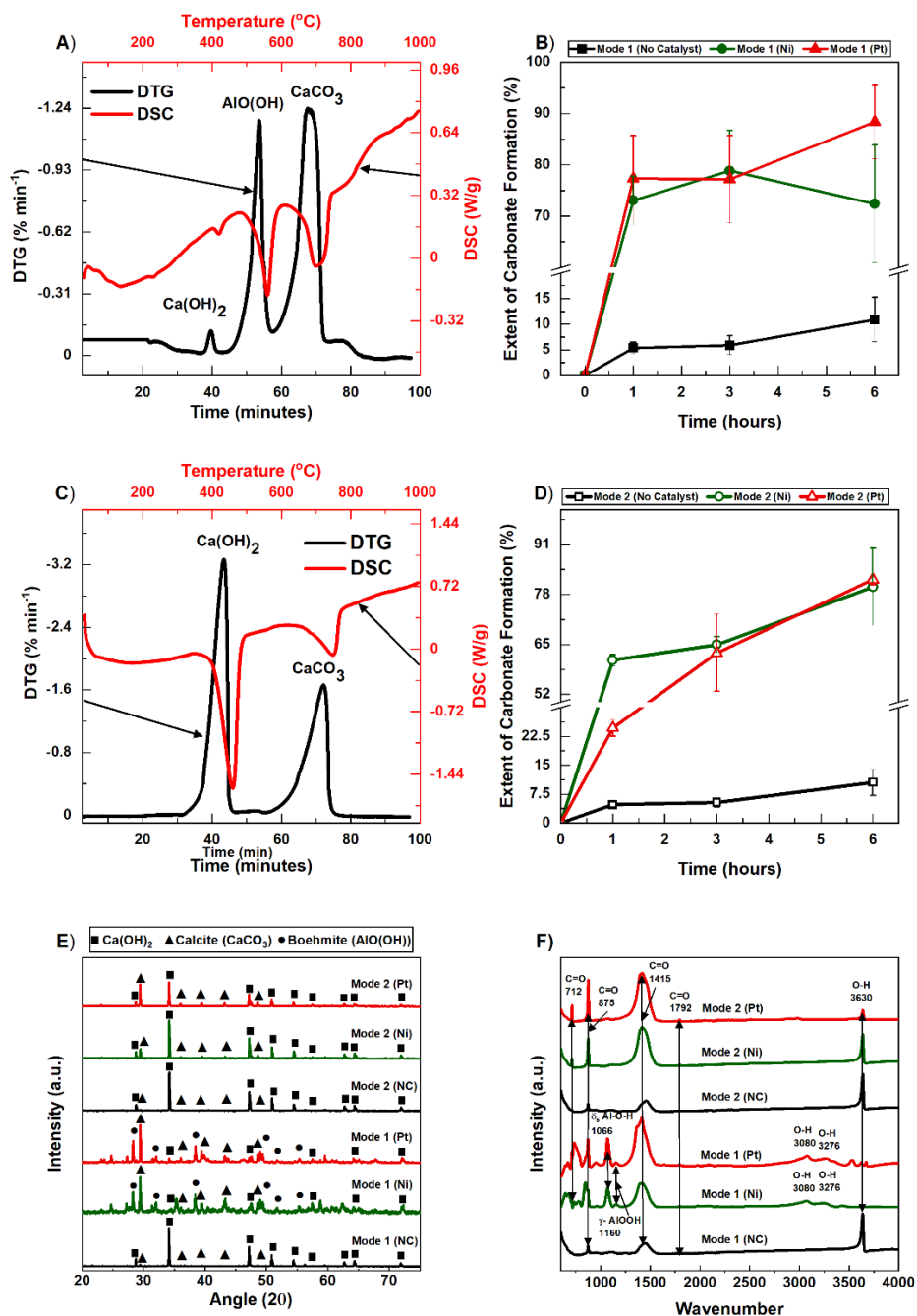
7
 8
 9



1

2 **Figure 3.** (a) Gas product yield for base case (without a catalyst) H₂ production from the
 3 hydrothermal treatment of 3 wt.% methanol with and without an alkaline sorbent (Ca(OH)₂). (b)
 4 H₂O Suppressed NMR spectra of liquid products from temporal evolution resulting from the
 5 deconstruction of oxygenates in the presence of alkaline sorbents in contact with fluid phase (Mode
 6 I). Only the dominant vibrations are labeled, and the spectra are offset for clarity. (c) Product yields
 7 in the gas phase when Ni/Al₂O₃ catalyst is used during the hydrothermal treatment of 3 wt.%
 8 methanol with and without an alkaline sorbent (Ca(OH)₂) (d) Product yields in the gas phase when
 9 Pt/Al₂O₃ catalyst is used during the hydrothermal treatment of 3 wt.% methanol with and without
 10 an alkaline sorbent (Ca(OH)₂). Alkaline sorbent reactions are carried out in Mode I (catalyst,
 11 sorbent and feedstock are mixed to form a slurry), and Mode II (sorbent is suspended in the gas
 12 phase, while the catalyst and feedstock are mixed in the liquid phase), at temperatures of 240 °C
 13 and pressures of 50 bar N₂ pressure. NA: No Alkalinity, NC: No Catalyst, M1: Mode I, and M2:
 14 Mode II.

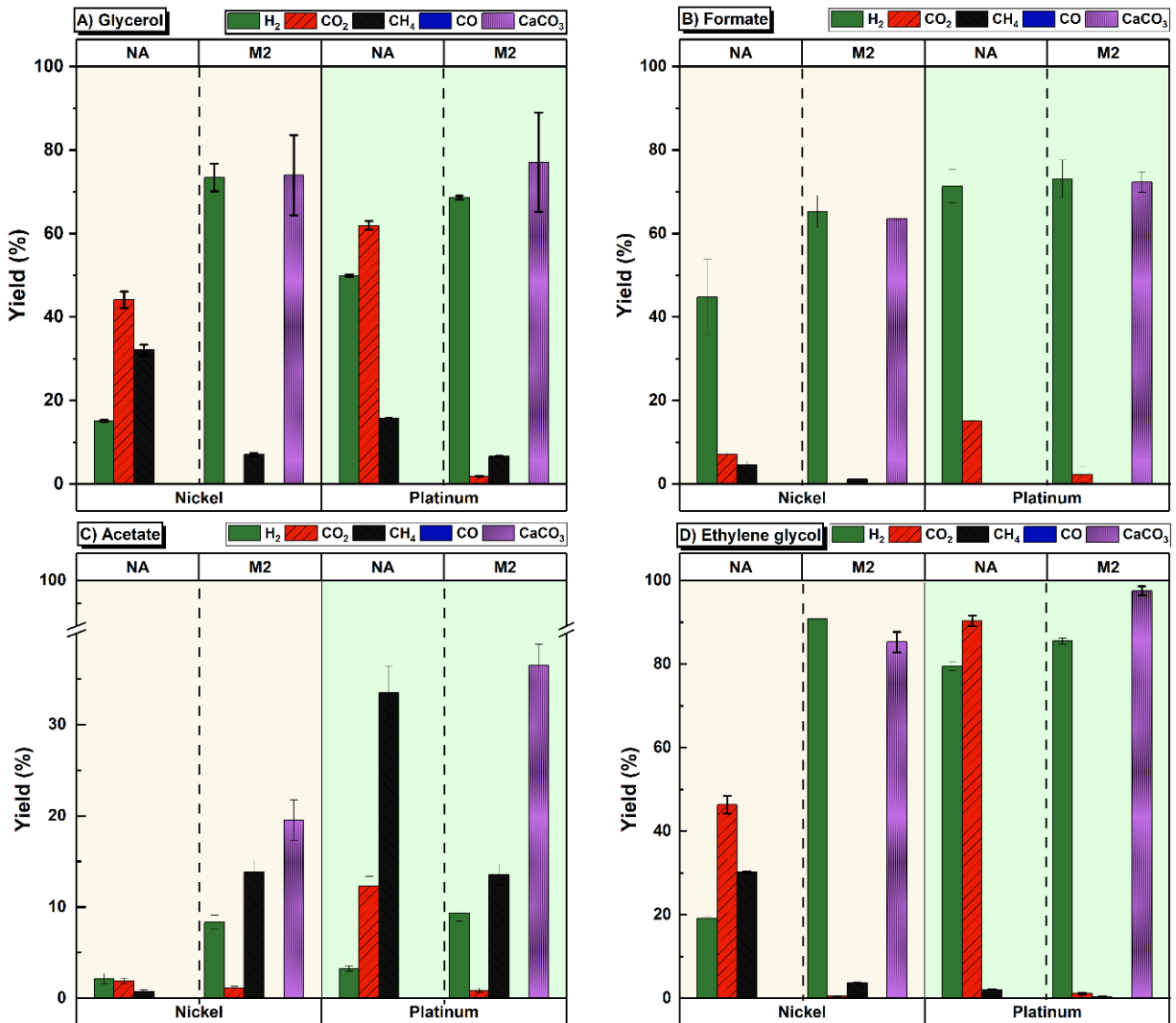
15



1

2 **Figure 4.** Evidence of calcium carbonate formation in the solid product obtained from H₂
 3 production via hydrothermal treatment of 3 wt.% methanol based on: (a) thermo gravimetric
 4 analysis of solid calcium carbonate product from Mode I, (b) calculated extent of calcium
 5 carbonate formation in solid product obtained from Mode I, (c) thermo gravimetric analysis of
 6 solid product from Mode II, (d) calculated extent of calcium carbonate formation in solid product
 7 obtained from Mode I, (e) XRD analyses showing calcium carbonate phases formed post-reaction,
 8 and (f) FTIR analyses of solid calcium carbonate products obtained post-reaction.

1



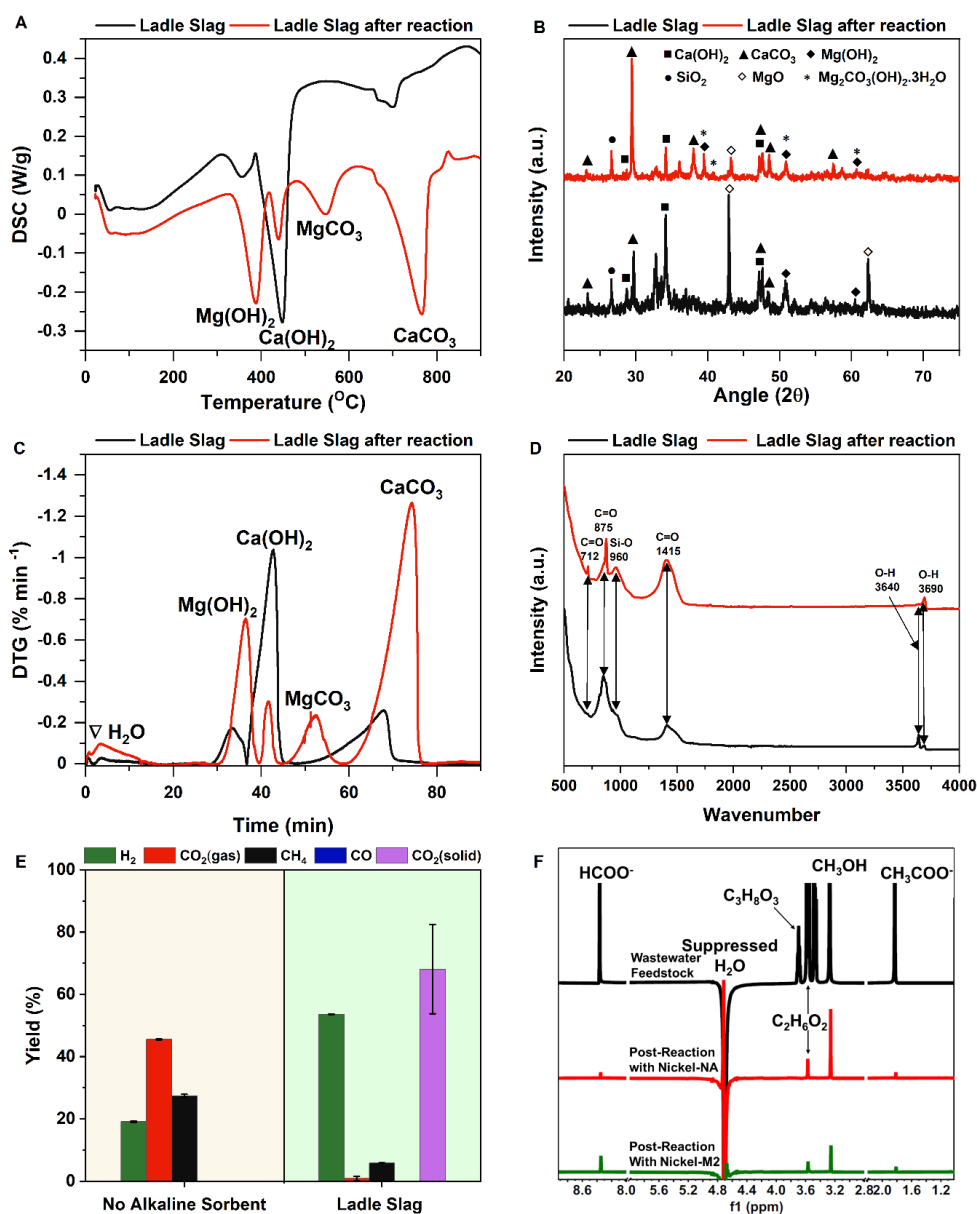
2

3 **Figure 5.** Yields of H₂, CO₂, CH₄, CO, and CaCO₃ resulting from the hydrothermal conversion of
 4 3 wt.% biomass oxygenates to H₂ with inherent carbon removal using Ca(OH)₂ sorbent where (a),
 5 (b), (c), and (d) represent glycerol, formate, acetate, and ethylene glycol, respectively. NA
 6 represents the scenario when there is no alkalinity in the system. M2 represents Mode II in which
 7 the alkaline sorbent is suspended in the gas phase, the catalyst and feedstock are mixed in the liquid
 8 phase, and the reaction temperature and N₂ pressure are 240 °C and 50 bar, respectively.

9

10

11

1
2

3

4 **Figure 6.** Contrasting unreacted and reacted ladle slag obtained after H₂ conversion from model
 5 wastewater and CO₂ removal from ladle slag with *in-situ* CO₂ capture using (a) DSC
 6 measurements, (b) XRD analyses, (c) DTG curves, (d) FTIR analyses, (e) product yields on using
 7 Ni/Al₂O₃ catalyst, and (f) H₂O suppressed NMR spectra of liquid products. Only the dominant
 8 vibrations are labeled, and the spectra are offset for clarity in (f). Reactions are carried out in Mode
 9 II where the sorbent is suspended in the gas phase, while Ni/Al₂O₃ catalyst and mixture of biomass
 10 oxygenates are mixed in the liquid phase, at temperatures of 240 °C and N₂ pressure of 50 bar.